environments

MDPI

Article

High-Performance Unpurified Food-Grade LBG/k-Carrageenan Antibacterial Films Functionalized with Pomegranate Peel Byproducts

Gianluca De Rinaldis [1,*], Giorgia Miccoli [1], Antonella Del Fiore [2], Chiara Nobili [2], Paolo Rotolo [1], Maurizio Notarfonso [2], Claudia Zoani [3] and Valerio Miceli [1,4]

[1] Laboratory for Innovation in Agrifood Supply Chains, Sustainable Agrifood Systems Division, Department of Sustainability, Circularity and Adaptation to Climate Change of Productive and Territorial Systems, National Agency for New Technologies, Energy and Sustainable Economic Development, Brindisi Research Center, SS 7 Appia Km 706, Cittadella della Ricerca, 72100 Brindisi, Italy; giorgia.miccoli@enea.it (G.M.); paolo.rotolo@enea.it (P.R.); valerio.miceli@enea.it (V.M.)

[2] Laboratory for Innovation in Agrifood Supply Chains, Sustainable Agrifood Systems Division, Department of Sustainability, Circularity and Adaptation to Climate Change of Productive and Territorial Systems, National Agency for New Technologies, Energy and Sustainable Economic Development, Casaccia Research Center, Via Anguillarese 301, 00123 Rome, Italy; antonella.delfiore@enea.it (A.D.F.); chiara.nobili@enea.it (C.N.); maurizio.notarfonso@enea.it (M.N.)

[3] Sustainable Agrifood Systems Division, Department of Sustainability, Circularity and Adaptation to Climate Change of Productive and Territorial Systems, National Agency for New Technologies, Energy and Sustainable Economic Development, Casaccia Research Center, Via Anguillarese 301, 00123 Rome, Italy; claudia.zoani@enea.it

[4] Department of Soil, Plant and Food Sciences (DiSSPA), University of Bari Aldo Moro, Via Amendola 165/A, 70126 Bari, Italy

* Correspondence: gianluca.derinaldis@enea.it; Tel.: +39-3289561569

Abstract

To address the challenges of persistent plastic pollution and food waste reduction, sustainable active packaging systems derived from renewable biopolymers represent alternative to non-renewable petroleum-based fossil plastics. In this context, an active, soil-biodegradable bio-packaging film was engineered via solvent casting from a synergistic binary blend of food grade carob seed flour (E410) and kappa-carrageenan (E407) plasticized with glycerol and functionalized with an aqueous extract from red pomegranate peel, a byproduct of pomegranate processing. The extract, recovered from this agricultural byproduct through ultrasound-assisted water extraction, exhibited rich phenolic, flavonoid, and anthocyanin contents together with strong radical scavenging capacity and broad-spectrum antibacterial activity against foodborne pathogens. When incorporated into the biopolymeric polysaccharide network, these bioactive constituents significantly enhanced tensile strength while maintaining high film flexibility and a hydrophobic surface character. The natural polyphenols were physically integrated into the matrix without disrupting the hydrocolloid framework. The functionalized films demonstrated antibacterial activity against Gram-positive and Gram-negative bacterial strains, good water vapor and gas barrier performance, and complete biodegradation in agricultural soil. Overall, this fully bio-based material demonstrates the technological potential of valorizing agro-industrial byproducts into high-performance active packaging capable of extending the shelf life of perishable food while aligning with circular bioeconomy frameworks.

Keywords: active food packaging; food-grade hydrocolloids; pomegranate peel polyphenols; green extraction; bioactive films; barrier properties; soil biodegradation; circular bioeconomy

Check for updates

Academic Editor: Joaquim Esteves Da Silva

Received: 4 October 2026
Revised: 24 October 2026
Accepted: 28 October 2026
Published: 30 October 2026

Copyright: © 2026 by the authors. Licensee MDPI, Basel, Switzerland. This article is an open access article distributed under the terms and conditions of the Creative Commons Attribution (CC BY) license.

1. Introduction

The global food sector faces the dual imperative of expanding production to meet escalating population demands while implementing advanced preservation strategies to ensure product safety, quality, and shelf-life extension without reliance on synthetic chemical additives [1,2]. Concurrently, the pervasive use of non-renewable, petroleum-based plastic packaging materials has generated severe environmental degradation and persistent plastic waste accumulation [3]. These critical challenges have catalyzed a technological shift toward sustainable active bio-packaging systems derived from renewable, eco-friendly biopolymers [4,5], and engineered to incorporate natural bioactive compounds that enhance food protection and extend shelf life. Such active materials not only serve as physical barriers against environmental contaminants but also actively interact with the packaged food matrix or headspace by releasing bioactive compounds capable of mitigating oxidative decay and suppressing microbial proliferation, thereby aligning directly with circular bioeconomy principles and food waste reduction frameworks [6].

Among natural biopolymers, plant and marine-derived polysaccharides, specifically galactomannans and sulfated galactans, have received substantial attention as continuous phase matrices for biodegradable film fabrication owing to their widespread abundance, non-toxicity, and excellent film-forming capacities [7,8]. Locust bean gum (LBG), isolated from the endosperm of carob (*Ceratonia siliqua* L.) seeds, is an almost neutral galactomannan [9,10]. Concurrently, k-carrageenan (k-car) is an anionic sulfated galactan extracted from red seaweeds, capable of assembling into rigid helical junction zones [11,12]. However, films formulated from individual biopolymers routinely exhibit inherent performance limitations, including high moisture sensitivity, poor water vapor barrier efficiency, and localized mechanical brittleness [13]. To overcome these drawbacks, the synergistic binary blending of structurally distinct hydrocolloids represents a highly effective strategy [14]. The physical association between the unsubstituted mannan regions of LBG and the double-helical domains of k-carrageenan establishes cohesive junction zones via extensive intermolecular hydrogen bonding networks [15,16]. This structural reinforcement improves film continuity, mechanical toughness, and gas containment properties [13,14].

Differing from the majority of the published literature relying on highly purified, analytical-grade biopolymers, this study employs commercial food-grade additives, specifically locust bean gum (E410) and kappa-carrageenan (E407), strictly compliant with food-grade legal standards. These cost-effective, food-grade raw materials naturally harbor intrinsic non-polymeric fractions, such as native proteins (just under 7% in E410) alongside residual sugars (<28%) and salt (10%) in E407. Rather than acting as inert impurities, these native co-constituents could actively participate in the supramolecular network architecture, contributing to enhanced cross-linking density, mechanical toughness, and gas/moisture barrier performance compared to pristine pure polymer matrices.

To convert these structural biopolymer networks into functional active packaging materials, the incorporation of bioactive phytocompounds isolated from agro-industrial byproducts offers a dual advantage: enhancing food preservation efficacy while valorizing low-cost agricultural side-streams [17–19]. Pomegranate (*Punica granatum* L.) processing generates substantial volumes of peel waste, accounting for up to 50% of the total fruit mass [18]. This exocarp tissue constitutes an exceptionally rich reservoir of bioactive secondary metabolites, dominated by hydrolysable tannins (such as punicalagin isomers and ellagic acid), phenolic acids (including protocatechuic, syringic, and iso-ferulic acids), and flavonoids [20–22]. These phytocompounds possess potent free-radical scavenging abilities and broad-spectrum antibacterial activity against key foodborne pathogens [23]. To isolate these thermolabile bioactive molecules efficiently and sustainably, green extraction technologies, particularly ultrasound-assisted extraction (UAE) utilizing pure water as a sol-

vent, have emerged as superior alternatives to conventional organic solvent extraction [24]. Acoustic cavitation induced by UAE disrupts the rigid plant cell wall matrix, enhancing solvent capillary penetration and mass transfer under mild thermal conditions, thereby preserving the intrinsic biological potential of the recovered extract [24].

When incorporated into the biopolysaccharide matrix, these natural polyphenols act as functional fillers and secondary hydrogen-bond donors [19,25]. This supramolecular association is hypothesized to increase effective cross-link density, reinforcing mechanical resistance, restricting matrix free volume for permeating gas molecules, providing sustained release of functional antioxidants and antimicrobials onto food surfaces [2]. Crucially, while non-covalent interactions enhance functionality during storage, they do not hinder environmental biodegradation, allowing the matrix to undergo rapid biotic mineralization in natural soil ecosystems [3].

In this context, national and European research infrastructures play a pivotal role in accelerating the transition toward sustainable agrifood systems by providing advanced analytical platforms, standardized methodologies, and open-access facilities and services (https://www.metrofood.eu/ accessed on 27 October 2026). Specifically, the METROFOOD-IT Research Infrastructure (Italian Research Infrastructure for Metrology and Open Access Data in Support to the Agrifood Mission), through its dedicated operational units and facilities located at the ENEA Research Centers of Brindisi and Casaccia (Italy), actively promotes circular bioeconomy frameworks also by driving the technological valorization of agri-food side-streams into high-performance functional biomaterials.

Therefore, within the strategic framework and experimental facilities of the METROFOOD-IT Research Infrastructure hosted at the ENEA Research Centers of Brindisi and Casaccia (Italy), the main objective of this study is to develop and characterize a novel, fully bio-based, and soil-biodegradable active packaging film based on a synergistic unpurified food grade LBG/k-carrageenan matrix functionalized with an aqueous extract of red pomegranate peel.

2. Materials and Methods

All processes, assays and characterizations were carried out using the equipment and physical facilities at the METROFOOD-IT Research Infrastructure located at the ENEA Research Centers of Brindisi and Casaccia (Italy).

2.1. Chemicals, Materials, and Instruments

Ethanol, glycerol (G5516), folin and Ciocalteu's phenol reagent (47641), 3,4,5-trihydroxybenzoic acid (gallic acid, G7384), 2,2-diphenyl-1-picrylhydrazyl radical (DPPH, D9132), (±)-6-hydroxy-2,5,7,8-tetramethylchromane-2-carboxylic acid (TROLOX, 238813), 7-hydroxy-3H-phenoxazin-3-one-10-oxide sodium salt (resazurin, R7017), 2-(3,4-dihydroxyphenyl)-3,5,7-trihydroxy-4H-1-benzopyran-4-one (quercetin, Q4951), sodium carbonate Na_2CO_3 (223530), round-bottom 96-well microplates, aluminum chloride $AlCl_3$ hexahydrate (237078), potassium acetate CH_3COOK (236497), and polypropylene containers were all purchased from Sigma-Aldrich (Merck Life Science s.r.l., Milan, Italy). Locust bean gum flour from ceratonia siliqua seeds (E410) and k-carrageenan (E407) were purchased from Gioia Group srl, Torino, Italy.

Acetic acid, chloridic acid, methanol, cyanidin-3-O-glucoside (C3G) with a molar extinction coefficient (26.900 $L \cdot mol^{-1} \cdot cm^{-1}$ 2690 m^2/mol) (PHL89616) and gentamicin sulfate (G1264), sterile blank paper discs, polystyrene Petri dishes, 0.45 µm PTFE (polytetrafluoroethylene) syringe filters and Whatman No. 1 filter papers were all purchased from Sigma-Aldrich (Merck Life Science s.r.l., Milan, Italy). Mueller–Hinton agar (MHA) and Mueller–Hinton broth (MHB) were obtained from Oxoid (Thermo Fisher Scientific,

Waltham, MA, USA). Ultra-pure distilled water was produced using a Milli-Q system. High-purity technical gases, including pure carbon dioxide, pure oxygen, and nitrogen/hydrogen carriers, were supplied by SIAD S.p.A (Bergamo, Italy).

The bacterial strains *Bacillus subtilis* (MTCC 5376), *Escherichia coli* (ATCC 25922), *Pseudomonas aeruginosa* (PA-01), and *Staphylococcus aureus* (ATCC 25923) were obtained from the Microbial Collection of ENEA (Italian National Agency for New Technologies, Energy and Sustainable Economic Development), Rome, Italy, registered in the SUS-MIRRI.IT network.

A Texture Analyzer TA.XTplus100C from Stable Micro System is used to evaluate the mechanical and tensile properties of the films; a Cary 630 ATR-FTIR analyzer and Agilent Infinity II 1260 Prime LC systems with Poroshell 120 EC-C18 from Agilent are used to perform FTIR-ATR spectroscopy and UHPLC-DAD chromatographic profiling; a Cary 50 UV-Vis spectrophotometer from Varian, Inc., measures absorbance in biochemical assays for polyphenols, flavonoids, anthocyanins, and DPPH antioxidant activity; a Nikon D7100 camera equipped with a Sigma 105 mm macro lens from Nikon and Sigma Corporation captures droplet images to determine the static water contact angle; a Sonica MH series ultrasonic bath from Soltec is used for ultrasound-assisted extraction and solution degassing; the Multiperm and PermO2 analyzers from Extra Solution s.r.l. measure the transmission rates and permeability of water vapor, carbon dioxide, and oxygen; an Alpha 1–2 LSCbasic laboratory freeze dryer from Martin Christ Gefriertrocknungsanlagen GmbH lyophilizes aqueous extracts to preserve thermolabile compounds; a thermostat-controlled air oven from Bicasa srl dries pomegranate peels and determines film moisture content; Peltier Constant climate chambers HPP110eco and HPP260eco from Memmert GmbH manage film conditioning and soil degradation tests; a Mixer Mill from Retsch GmbH grinds samples into fine powders; a high-speed refrigerated centrifuge from Beckman Coulter separates liquid and solid phases after extraction; a digital high-precision micrometer from Mitutoyo measures film thickness; a digital caliper from Borletti measures inhibition zone diameters in antimicrobial tests; and a vortex mixer from Velp Scientifica rapidly homogenizes mixtures during sample preparation.

2.2. Red Pomegranate Sampling

Red pomegranate (*Punica granatum* L.) fruits of the "Wonderful One" cultivar were hand-harvested in 2025 from different trees at a local farm, Azienda Agricola Durante (40.235198, 17.933207), in Nardò (Lecce, Italy). Subsequently, the fruits were immediately transported to the ENEA-IFAL (Brindisi-IT) and washed with distilled water. The nine harvested fruits were divided into three experimental groups of three fruits each (Group/Pool 1: Samples 1–3; Group/Pool 2: Samples 4–6; Group/Pool 3: Samples 7–9). Each fruit was processed individually to separate the peel from the kernels and mesocarp (albedo), allowing individual tracking of morphometric parameters and drying yields across all nine samples. The individual peels were oven-dried at 45 °C for 5 days [26] and subsequently ground into fine powders. Based on these gravimetric measurements, the calculated peel moisture content (%) was expressed on a wet weight basis according to the following equation:

$$\text{Moisture Content (\%)} = ((\text{Fresh Peel Weight} - \text{Dry Peel Weight})/\text{Fresh Peel Weight}) \times 100$$

2.3. Sequential Extraction and Lyophilization

The aqueous extracts were prepared from each of the nine dried peel samples (Samples 1–9) using a triple sequential ultrasound-assisted extraction (UAE) process [24,27] to evaluate extraction yields and mass balances individually. For each cycle, powdered peel from an individual sample was mixed with 1:20 (w/v) distilled water at 45 °C and vortexed

for 15 s to ensure thorough homogenization. The mixture was then subjected to ultrasonic waves (40 kHz) for 15 min [28,29]. Following each sonication cycle, the suspension was centrifuged at 4000× *g* for 5 min to facilitate liquid phase separation. The resulting supernatants were collected, filtered through Whatman No. 1 paper, combined, centrifuged at 4000× *g* for 15 min, and lyophilized to preserve thermolabile bioactive compounds. Subsequently, equal proportions of the lyophilized extracts from each group of three samples were pooled together to yield three final representative red pomegranate peel aqueous extract pools (Pool 1, Pool 2, and Pool 3), which served as independent biological replicates for subsequent biochemical, antimicrobial, and film characterization assays. The final R3PAE lyophilized samples were stored at −20 °C until further use.

2.4. Biochemical Characterization of the Extract

Polyphenols Extraction

The extraction method followed the general principles reported by Luque Rodríguez et al. (2006) [30], employing ethanol–water mixtures for polyphenol recovery from plant tissues. In detail, the extraction was carried out by weighing 100 mg of freeze-dried material and mixing it with 2 mL of 80% ethanol in conical tubes. The samples were incubated in a water bath at 80 °C for 30 min under gentle agitation, followed by centrifugation at 10,000 rpm/11,644× *g* for 10 min. The supernatant was collected and filtered through 0.45 µm PTFE syringe filters; the resulting extracts were subsequently used for the determination of total polyphenols, flavonoids, and antioxidant activity.

Total Phenolic Content (TPC)

The total phenolic content (TPC) of the R3PAE was determined using the Folin–Ciocalteu colorimetric method, as described by Emmons et al. (1999) [31], with some modifications. Briefly, 0.078 mL of the diluted R3PAE was mixed with 0.078 mL of Folin–Ciocalteu reagent (previously diluted 1:10, *v*/*v*) and 1.25 mL of deionized water. The mixture was shaken and incubated in the dark at room temperature for 7 min. Subsequently, 0.157 mL of a 20% (*w*/*v*) sodium carbonate (Na_2CO_3) solution was added to the mixture. After an additional incubation period of 40 min at room temperature in the dark, the absorbance was measured at 725 nm against a reagent blank using a UV–Vis spectrophotometer. A calibration curve was constructed using serial dilutions of the gallic acid (3,4,5 trihydroxybenzoic acid) standard, preparing solutions at 500, 350, 250, 100, 50, 25 and 10 mg/L. The results were expressed as milligrams of gallic acid equivalents per gram of dry weight (mg GAE/g DW). All analyses were performed in triplicate, and data were expressed as the mean ± standard deviation.

Total Flavonoids Content (TFC)

The total flavonoid content (TFC) of the R3PAEs was determined using the aluminum chloride hexahydrate colorimetric assay, according to the method of Win et al. (2019) [32], with minor modifications. Briefly, 0.2 mL of the diluted R3PAE was mixed with 0.6 mL of 95% (*v*/*v*) ethanol, 0.040 mL of 10% (*w*/*v*) aluminum chloride hexahydrate, 0.040 mL of 1 M potassium acetate solution, and 1.120 mL of distilled water. The mixture was vortexed and incubated at room temperature in the dark for 30 min. The absorbance of the reaction mixture was measured at 415 nm against a blank. A calibration curve was prepared using serial dilutions of the flavonoid quercetin as the reference standard, at concentrations of 100, 75, 50, and 25 µg/mL. The total flavonoid content was expressed as milligrams of quercetin equivalents per gram of dry weight (mg quercetin equivalents per g DW). All measurements were performed in triplicate, and the data were expressed as the mean ± standard deviation.

Anthocyanin Extraction and Quantification

Anthocyanin extraction was carried out following the method described by Iland et al. (1996) [33]. Briefly, 0.02 mg of the sample was transferred into a 15 mL plastic centrifuge

tube. Subsequently, 2 mL of 50% (v/v) aqueous ethanol was added to the homogenate portion. The tube was securely capped and agitated on a mixing device for 1 h, ensuring efficient mixing to prevent the pellet from becoming lodged or settling at the bottom of the tube. To separate the solid plant debris from the liquid phase, the mixture was then centrifuged at a relative centrifugal force of 1800× g for 10 min, and the resulting liquid supernatant containing the dissolved anthocyanins was collected as the extract. As for the extraction, the total anthocyanin content was also determined using the method described by Iland et al. (1996) [33], with specific modifications. For color development, a 100 µL aliquot of this extract was transferred to a tube, diluted with 1.9 mL of 1.0 M HCl, and incubated at room temperature for at least 3 h to allow full expression of color. The absorbance of the acidified solution was measured at 520 nm using a UV–Vis spectrophotometer against a reagent blank consisting solely of 1.0 M HCl. The final concentration was calculated using the molar extinction coefficient (26.900 $L \cdot mol^{-1} \cdot cm^{-1}$/2690 m^2/mol), which defines the specific light-absorption capacity per unit of concentration and path length according to the Beer–Lambert law of cyanidin-3-O-glucoside (C3G) evaluated in the same solvent. All analyses were performed in triplicate, and data were expressed as the mean ± standard deviation.

DPPH Radical Scavenging Activity Evaluation

The DPPH radical scavenging activity of the R3PAEs was determined spectrophotometrically according to the method described by Li et al. (2010) [34], with some modifications. Briefly, the lyophilized R3PAE was redissolved and appropriately diluted in 80% (v/v) ethanol. An aliquot of 0.040 mL of the diluted extract was mixed with 1.16 mL of a 0.06 mM DPPH working solution. The mixture was shaken thoroughly and allowed to stand at room temperature in the dark for 30 min. The absorbance of the reaction mixture was then measured at 515 nm using a UV–Vis spectrophotometer against an ethanol blank. Trolox was employed as the reference standard, and a calibration curve was prepared using serial dilutions of synthetic analog of vitamin E Trolox (6-hydroxy-2,5,7,8-tetramethylchroman-2-carboxylic acid) (750 µM, 500 µM, 250 µM, 100 µM, 50 µM). The radical scavenging capacity was calculated from the decrease in absorbance and expressed as milligram of Trolox equivalents per gram of dry weight (mg of Trolox equivalents per g DW). All measurements were performed in triplicate, and the data were expressed as the mean ± standard deviation.

Chromatographic Profiling with UHPLC-DAD

To establish the qualitative phytochemical profile of R3PAE, an Ultra-High-Performance Liquid Chromatography system equipped with a Diode Array Detector (UHPLC-DAD) was employed. Chromatographic separation was carried out on a C18 reversed-phase column following a method modified from El-Hamamsy & El-Khamissi (2020) [20]. The mobile phase consisted of methanol, water, and acetic acid (24:75:1, $v/v/v$) at a flow rate of 1.0 mL/min, with UV detection monitored at 280 nm. The resulting chromatographic profile was qualitatively compared with established literature data on pomegranate extracts to evaluate overall sample complexity and key fingerprint features, without pursuing individual compound identification or quantification.

2.5. Antimicrobial Evaluation of the R3PAE Extract and Determination of Film Loading Concentration

Minimum Inhibitory Concentration (MIC) Evaluation

The antimicrobial activity of the R3PAE was determined by the broth microdilution method using resazurin as a metabolic indicator to assess cell viability. The protocol first developed by Elshikh et al. (2016) [35] for biosurfactants was successfully adapted with minor modifications for R3PAE, preparing serial two-fold dilutions in a 96-well microplate covering a final concentration range from 20 to 0.625 mg/mL with a final volume of 100 µL.

The bacterial suspensions were prepared following standardized guidelines. Briefly, bacterial strains *Bacillus subtilis* (MTCC 5376), *Escherichia coli* (ATCC 25922), *Pseudomonas aeruginosa* (PA-01), and *Staphylococcus aureus* (ATCC 25923) were streaked and grown on Mueller–Hinton agar (MHA) plates at 37 °C for 24 h. Fresh colonies were suspended in sterile saline solution (0.9% NaCl), and the turbidity was adjusted to match the 0.5 McFarland standard (approximately 1.5×10^8 CFU/mL). This suspension was then diluted in Mueller–Hinton broth (MHB) to achieve a final inoculum concentration of approximately 10^5 CFU/mL in each test well.

Each well was inoculated accordingly, and after incubation at 37 °C for 24 h, 30 µL of a sterile resazurin solution (0.015%, *w*/*v*) was added to each well, and the plates were further incubated for at least 2 h and up to 4 h depending on the bacterial strain.

The MIC was defined as the lowest concentration of the extract that prevented the color change of resazurin from blue to pink, indicating complete inhibition of bacterial growth. All assays were conducted in triplicate, including positive (gentamicin antibiotic), negative (growth medium only), and extract only controls. To account for background color interference at high extract concentrations ≥ 20 mg/mL, dual-wavelength absorbance was recorded at 570 nm and 605 nm using a microplate reader.

Disc Diffusion Assay for Determination of Film Loading Concentration

The antimicrobial efficacy of the R3PAE extract was preliminarily screened using the agar disc diffusion method [36] with minor adaptation to guide the formulation and rational loading of the active films. Briefly, bacterial overnight cultures of *Bacillus subtilis* (MTCC 5376), *Escherichia coli* (ATCC 25922), *Pseudomonas aeruginosa* (PA-01), and *Staphylococcus aureus* (ATCC 25923) were suspended in sterile saline solution and adjusted to a turbidity equivalent to a 0.5 McFarland standard. These standardized suspensions were uniformly spread across the surface of Mueller–Hinton agar plates using sterile cotton swabs in three directions to ensure a confluent bacterial lawn. Sterile blank paper discs (diameter of 6 mm) were then impregnated with a constant volume (6 µL) with different amounts of compound each (ranging from 0.25 to 10 mg) of the R3PAE dissolved in water solvent. Discs loaded with the solvent alone and with gentamicin were used as negative controls and positive controls, respectively. All discs were allowed to dry completely under a laminar flow hood to prevent solvent-induced diffusion artifacts before being aseptically placed onto the inoculated agar surface. After an incubation period of 24 h at 37 °C, the antimicrobial activity was evaluated by measuring the total diameter of the clear inhibition zones (including the disc diameter) in millimeters using a digital caliper. To ensure accuracy, each inhibition zone was measured in two perpendicular directions, and the average value was recorded. All data were expressed as the mean ± standard deviation.

2.6. Film Fabrication via Solvent Casting

Films were prepared via a modified solvent casting technique based on the synergistic blend of food-grade E410 locust bean gum (LBG) and E407 kappa-carrageenan (k-car), adapting the protocol described by Pinheiro et al. (2011) [15] and improved by Martins et al. (2012) [14] with some modifications related to the concentration, temperature, degassing system, and the amount of glycerol. In particular, the utilization of commercial E410 and E407 raw materials, incorporating native protein (<7%), sugar (<28%) and salt (10%) components within food-grade legal limits, required specific adjustments in thermal activation (80 °C for 1 h) and glycerol plasticizer loading (0.75% *w*/*v*) to ensure full dispersion and optimal macromolecular interaction.

Briefly, the polysaccharides, LGB and k-car, were dispersed in distilled water with a ratio of 60/40 and at a total polymer concentration of 1% and stirred for at least 1 h at room temperature to ensure complete hydration. The dispersion was then heated to 80 °C

under constant agitation for 1 h to induce complete thermal activation and solubilization of the macromolecular chains. Glycerol was chosen as a plasticizer and incorporated at a concentration of 0.75% (w/v) relative to the total volume of solution, and the solution was stirred for 1 h until fully blended. Then, the solution was cooled to 40 °C, avoiding the premature gelation of the polysaccharide matrix, and the lyophilized R3PAE was weighted and incorporated into the mixture to obtain the bioactive film version. A control film was also prepared following the same procedure but without the addition of the R3PAE extract. Both active and control film forming solutions were stirred using a magnetic stirrer for 30 min to ensure homogeneity and then subjected to an ultrasound bath treatment (using a Soltec Sonica MH series bath operating at 40 kHz) for 30 min at a controlled temperature of 40 °C to reduce degassing (microbubbles). To guarantee high reproducibility and maintain a constant film thickness, a standardized volume of each solution was cast onto leveled dishes by maintaining a fixed volume-to-surface area ratio (200 mL × 300 cm^2). Then, the leveled dishes were dried in a constant temperature and humidity chamber set at 45 °C and 15% relative humidity (RH) for 24 h. Finally, the resulting dry films were peeled off and placed in a constant temperature and humidity chamber under controlled conditions (25 °C and 54% RH for 3 days) for final conditioning prior to further characterization. The entire preparation process was repeated in three independent sessions to obtain at least three replicates each time for both the control and the bioactive film versions.

2.7. Diffusion Assay for Films Antimicrobial Evaluation

The antimicrobial efficacy of the developed bioactive films was evaluated using the agar diffusion method adapting the protocol of disc diffusion assay [36]. Briefly, bacterial inocula of *Bacillus subtilis* (MTCC 5376), *Escherichia coli* (ATCC 25922), *Pseudomonas aeruginosa* (PA-01), and *Staphylococcus aureus* (ATCC 25923) were prepared by suspending overnight cultures in sterile saline solutions to match the turbidity of a 0.5 McFarland standard. These standardized suspensions were spread over the surface of Mueller–Hinton agar plates using sterile swabs to ensure a completely confluent bacterial lawn. Square specimens of the active films 5 mm × 5 mm, surface area of 0.25 cm^2, were aseptically cut and carefully placed onto the inoculated agar surface, ensuring intimate and uniform contact between the film matrix and the medium to facilitate proper hydration and subsequent diffusion of the active compounds. For comparison, control films prepared without R3PAE and standard antibiotic discs containing gentamicin were tested under identical conditions on the same plates to assess any inhibitory effects from the polymer matrix itself and as positive control to compare the films antimicrobial efficacy. The plates were then incubated at 37 °C for 24 h. The antimicrobial activity was quantified by measuring the total diameter of the clear inhibition zone surrounding each square film (including the film) in millimeters using a caliper. All three experiments were performed in triplicate, and the results were reported as the mean value of three independent experiments with three replicates ± standard deviation.

2.8. Fourier-Transform Infrared Spectroscopy (FTIR-ATR)

Potential structural alterations and intermolecular chemical interactions between the biopolymer matrix and the R3PAE were investigated via Fourier-Transform Infrared Spectroscopy coupled with Attenuated Total Reflection (FTIR-ATR). Spectra were acquired using an ultra-compact Agilent Cary 630 FTIR spectrometer equipped with a single-reflection diamond ATR accessory. The analyses were performed in the spectral range of 4000–650 cm^{-1} at a spectral resolution of 4 cm^{-1}, accumulating 64 scans per spectrum to optimize the signal to noise ratio. A background spectrum of the clean diamond crystal against air was collected prior to each measurement. The resulting spectra were evaluated to monitor the

characteristic absorption bands corresponding to both the polysaccharide backbone and the phenolic constituents of the incorporated extract.

2.9. Mechanical and Physical Characterization

Film Thickness and Moisture Content

The thickness of the films, both the control and the bio active version were determined using a high-precision electronic micrometer IP54 DIN 863 (resolution 0.001 mm; 0–25 mm). To account for any localized variations and ensure representative data, between five to 10 replicate measurements were performed at randomly selected positions across the surface of each film specimen. The moisture content of the films was evaluated using a gravimetric approach [37]. Film samples were weighed and were dried at 105 °C in a thermostat-controlled air oven (BICASA) until a constant weight was achieved (24 h). The moisture was subsequently calculated based on the weight loss of the samples before and after the drying process. All preparations and analyses were performed across three independent experimental sessions, with each session including triplicate samples. For each film specimen, thickness data represent the average of five to 10 random measurements. All resulting data for both thickness (five to 10 measurements each sample) and moisture content were expressed as the mean ± standard deviation in triplicate and utilized as baseline parameters for subsequent evaluations.

Mechanical Properties of the Films

The tensile properties of the films were evaluated in accordance with the ASTM D-882 [38] standard method using a texture analyzer equipped with a 100 N load cell and tensile grips. Prior, in accordance with ASTM D-882 standard [38], films were cut into rectangular strips with a width of 6 mm and a length of 50 mm using a preformed template. The initial grip separation (gauge length, L0) was constant for all the measurements, and the crosshead speed was maintained constant until film rupture occurred; again both values were set following the parameters of the ASTM D-882 standard [38]. From the resulting load extension curves, the following mechanical parameters were determined: Force at Break (F, g): extracted directly as the maximum load recorded at the exact point of specimen failure; Elongation at Break (EB, %): calculated as the mm and percentage change in film length relative to the initial gauge length using the following equation:

$$(\text{EB } \%) = \Delta L \backslash L0 \times 100$$

where ΔL represents the extension at the moment of rupture (mm) and L0 is the initial grip separation (mm).

To ensure cross-sectional accuracy for stress calculations, the individual thickness of each strip was measured prior to execution. A minimum of three specimens were tested for each film formulation (control film and R3PAE film), and the results were reported as mean values ± standard deviation.

Surface Hydrophobicity and Water Contact Angle (WCA)

The surface hydrophobicity of the films was evaluated by measuring the static water contact angle (WCA) through the sessile drop method, utilizing a custom-designed optical acquisition system. To prevent any localized curling or wrinkling and ensure a perfectly level testing surface, each film specimen was securely tensioned between two mechanical grips. A droplet of distilled water (10 μL) was carefully deposited onto the horizontal film surface using a precision micropipette, in accordance with the protocol described by ASTM D7334 [39]. A digital single-lens reflex (DSLR) Nikon D7100 camera on a tripod with remote control and equipped with a Sigma 105 mm F2.8 macro lens was aligned horizontally and manually focused on the drop point of the film plane and fixed at almost the minimum distance. To allow for initial droplet stabilization and achieve thermodynamic

equilibrium, a short sequence of high-resolution digital images was captured 5 s after deposition with built-in camera features (jpeg, 6 fps, about 5 s). Between the resulting images, the best images were chosen and subsequently analyzed using ImageJ (Version 1.54t 16 May 2026) software (National Institutes of Health, USA) equipped with the Contact Angle plugin [40], which calculated the contact angle at the liquid solid air interface by fitting the droplet profile using a sphere approximation with five points. All measurements were performed under standard laboratory conditions (controlled room temperature of 23 °C, relative humidity of 60%, and normal atmospheric pressure), in compliance with ASTM guidelines, to ensure the reproducibility and comparability of the results. At least three replicate measurements were conducted at different random positions on each film formulation (both the control and the activated film), and the results were reported as mean values ± standard deviation.

Water Vapor Transmission Rate and the related Permeability

The water vapor barrier properties of the films were determined using an automated MultiPerm 065 permeabilimeter (Extra Solutions, Pisa, Italy) equipped with an electrolytic detection sensor (P2O5), in accordance with the ASTM F1249 standard [41]. The film specimens were securely blocked into the circular permeation testing area, providing an active analysis surface area of 50 cm^2. Testing was conducted at a strictly controlled setpoint temperature of 23 °C. Prior to the automated measurement, the samples were subjected to an initial equilibration phase under the instrument's 'medium conditioning' mode to ensure matrix stabilization. A constant carrier gas flow rate of 13 mL/min was maintained throughout the analysis. The instrument monitored the moisture flux until a steady state profile was achieved, directly quantifying the final Water Vapor Transmission Rate (WVTR) expressed in $g/m^2 \times 24$ h. To account for geometric variations, the Water Vapor Permeability (WVP, $g \cdot m^{-1} \cdot s^{-1} \cdot Pa^{-1}$) was subsequently calculated by normalizing the steady state WVTR against the average film thickness (d, m) and the water vapor partial pressure differential (ΔP, Pa) across the film, according to the following equation:

$$WVP = WVTR \times D/\Delta P$$

All analyses were performed in triplicate, and the final barrier parameters were reported as mean values ± standard deviation.

Carbon Dioxide Transmission Rate CO_2TR and Permeability CO_2P

The carbon dioxide (CO_2) barrier properties of the films were evaluated using the same automated MultiPerm permeabilimeter (Extra Solutions, Pisa, Italy), which is equipped with a non-dispersive infrared (NDIR) detector, in accordance with the ASTM F2476 standard [42]. The film specimens were securely blocked into the permeation testing cells, providing an active analysis surface area of 50 cm^2. Testing was performed at a strictly controlled setpoint temperature of 23 °C under dry conditions. Prior to measurement, the samples underwent an initial conditioning phase under medium conditioning mode to ensure matrix stabilization. Pure CO_2 gas was introduced into the upper chamber of the cell, while a constant carrier gas flow was maintained in the lower chamber to convey the permeated gas to the infrared sensor. The instrument monitored the gas flux until a steady-state profile was achieved, directly quantifying the final Carbon Dioxide Transmission Rate (CO_2TR) expressed in $cm^3/m^2 \times 24$ h. The Carbon Dioxide Permeability (CO_2P, $cm^{3STP} \cdot m \cdot m^{-2} \cdot s^{-1} \cdot Pa^{-1}$) was subsequently calculated by converting the CO_2TR time base from 24 h to seconds and normalizing the steady-state flux against the average film thickness (d, m) and the CO_2 partial pressure differential (ΔP, Pa) across the film, according to the following equation: $CO_2P = (CO_2TR/86400) \times d/\Delta P$. All analyses were performed in triplicate, and the final barrier parameters were reported as mean values ± standard deviation.

Oxygen Transmission Rate OTR and Permeability OP

The oxygen O_2 barrier performance of the developed films was determined using an automated PermO_2 permeabilimeter (Extra Solutions, Pisa, Italy) equipped with a high sensitivity coulometric sensor, according to the ASTM D3985 standard [43]. The film specimens were placed into the testing cells, providing an active analysis surface area of 50 cm^2, and evaluated at a constant setpoint temperature of 23 °C under dry conditions. After an initial conditioning and purging phase with a nitrogen/hydrogen carrier gas to eliminate residual oxygen and stabilize the sample matrix, pure oxygen gas was introduced into the test chamber. The carrier gas swept the lower chamber, directing the permeated oxygen molecules toward the coulometric detector. The measurement proceeded until the oxygen flux reached a steady-state condition, yielding the Oxygen Transmission Rate OTR expressed in $cm^3/(m^2 \times 24\ h)$. The Oxygen Permeability OP, $cm^{3STP} \cdot m \cdot m^{-2} \cdot s^{-1} \cdot Pa^{-1}$, was then calculated by normalizing the steady-state OTR against the average film thickness (d, m) and the oxygen partial pressure gradient (ΔP, Pa) across the specimen, using the following equation: $OP = OTR \times d/\Delta P$. All measurements were conducted in triplicate, and the results were expressed as mean values ± standard deviation.

2.10. Soil Burial Degradation Assay

The environmental impact and the aerobic biodegradability of the films was evaluated through a simple soil burial degradation test conducted in a climate-controlled chamber following Alves et al. (2024) [44], with minor modification. Briefly, film specimens (20·20 mm) were weighed to determine their initial dry mass (Wi) and placed inside polypropylene containers to facilitate specimen recovery while ensuring direct contact with the soil microbiota. The samples were buried at a depth of 2 cm in natural agricultural soil (pH 7.2, characterized by a loose, highly porous, and fibrous texture, with a C/N ratio of approximately 12:1, comprising an organic carbon content of 25–30%, total nitrogen of 1.5–2.5%, and phosphorus around 1% on a dry weight basis) that had been sieved through a 2 mm mesh to remove debris. The containers were maintained in a climate chamber at a constant temperature of 25 °C and a relative humidity (RH) of 60% in the absence of light. To ensure optimal microbial activity and a high degree of biodegradation, the soil moisture content was set and strictly maintained at 60% of its water-holding capacity throughout the experiment by periodically monitoring container weights and adding distilled water as necessary.

Degradation was monitored over a period of 30 days, and at specific time intervals (0, 7, 14, 21, and 30 days), triplicate samples for both the active R3PAE films and the control films were carefully retrieved, gently cleaned with a soft brush to remove adhering soil particles, and dried in a vacuum desiccator until a constant mass was reached. The degree of degradation was quantified through visual inspection (digital photography) and gravimetric analysis, with the percentage of weight loss (WL %) calculated using the following equation: $WL\ \% = (Wi - Wt)/Wi \times 100$, where Wi is the initial dry mass of the film and Wt is the dry mass of the residual film at time t. All experiments were performed in triplicate to ensure statistical significance, and the results were expressed as mean values ± standard deviation.

3. Results

3.1. Fruit Characterization and Pomegranate Peel Powder Yields

To ensure uniformity and standardization before the extraction phase, parameters of the harvested *Punica granatum* L. (cultivar "Wonderful One") fruits were systematically evaluated. The cumulative fresh weight for all nine processed fruits was 3646.31 g, with an overall mean fruit mass of 405.15 ± 26.96 g. The manual separation of the exocarp from the edible portion yielded a total fresh peel biomass of 540.95 g, which corresponds to an average fresh peel weight of 60.07 ± 4.72 g per single fruit. Overall, the fresh peel portion

accounted for 14.83 ± 0.28% of the total fruit weight. Following the preparation of the Red Pomegranate Peel Pools (RPPPs), the oven drying process at 45 °C for 5 days resulted in a stable dry matrix, providing a mean overall yield of 39.41% relative to the initial fresh peel weight. Subsequently, the dried peels were ground using a laboratory grinder into a fine powder to maximize the efficiency and surface area for the subsequent extraction process. Comprehensive morphometric data, pool specific distributions, and individual dry matter yields are reported in Table 1.

Table 1. Morphometric characteristics, dry matter yields, and calculated peel moisture content of red pomegranate (*Punica granatum* L.) fruits and peel pools. Values are expressed as individual measurements and mean ± standard deviation (SD).

Pool/Sample ID	Sample Fresh Weight (g)	Total Fresh Weight (g)	Mean Sample Weight (g)	Fresh Peel Weight (g)	Fresh Peel Ratio (%)	Dry Peel Weight (g)	Dry Peel Yield (%)	Calculated Peel Moisture Content (%)
Pool 1								
Sample 1	412.48	—	—	61.25	14.85	22.58	36.87	**63.13**
Sample 2	447.15	—	—	67.88	15.18	25.42	37.45	**62.55**
Sample 3	441.02	—	—	66.11	14.99	24.65	37.29	**62.71**
Pool Summary	**—**	**1300.65**	**433.55 ± 18.50**	**195.24**	**15.01**	**72.60**	**37.23**	**62.77 ± 0.30**
Pool 2								
Sample 4	358.21	—	—	51.85	14.47	20.12	38.80	**61.20**
Sample 5	393.44	—	—	57.12	14.52	22.15	38.78	**61.22**
Sample 6	399.76	—	—	57.81	14.50	22.41	38.76	**61.24**
Pool Summary	**—**	**1150.41**	**383.47 ± 22.04**	**166.78**	**14.50**	**64.68**	**38.78**	**61.22 ± 0.02**
Pool 3								
Sample 7	388.15	—	—	58.12	14.97	24.62	42.36	**57.64**
Sample 8	407.62	—	—	61.05	14.98	25.92	42.46	**57.54**
Sample 9	399.48	—	—	59.76	14.96	25.30	42.34	**57.66**
Pool Summary	**—**	**1195.25**	**398.42 ± 9.78**	**178.93**	**14.97**	**75.84**	**42.39**	**57.61 ± 0.06**
Overall/Mean	**—**	**3646.31**	**405.15 ± 26.96**	**540.95**	**14.83 ± 0.28**	**213.17**	**39.41**	**60.59 ± 2.31**

Values are expressed as direct experimental measurements and mean ± standard deviation (SD).

Regarding the moisture content, the fresh pomegranate peel exhibited a mean moisture content of 60.59 ± 2.31%, corresponding to the average dry peel yield reported above. Gravimetric tracking across the three experimental batches demonstrated high consistency, with the individual moisture values reported in Table 1. These values fall just below the typical physiological range (64–74%) reported for pomegranate rind cultivated under Mediterranean climatic conditions [45]. Furthermore, this value is approximately 15 percentage points lower than that reported by Montefusco et al. (2021) [21] for the same cultivar grown in a different farm within the same geographical area. This divergence suggests that agricultural management, specifically dry farming or dryland cultivation techniques, alongside specific weather conditions during the growing period, may significantly influence the final moisture status of the fruit. Overall, the relatively low initial moisture content observed reflects an optimal fruit ripening stage at harvest, providing a dense solid matrix highly suitable for bioactive compound extraction.

The standardized fine powders obtained were subsequently utilized as the starting material for the triple sequential ultrasound-assisted extraction (UAE) and lyophilization processes to successfully isolate the stable, concentrated R3PAE powder.

3.2. Sequential Extraction Yields and Mass Balance Optimization

The triple sequential ultrasound-assisted extraction (UAE) process, followed by lyophilization, demonstrated high efficiency and reproducibility in isolating water-soluble compounds from the dried Red Pomegranate Peel Pools (dRPPPs). Across all nine individual samples, the protocol achieved a grand mean extraction yield of 54.742 ± 1.527%, corresponding to an average recovery of 0.548 ± 0.016 g of solid R3PAE powder per gram of dry peel matrix. The mean extraction yield remained highly consistent across the three sample groups, averaging 55.176 ± 2.623% for Pool 1 (Samples 1–3), 54.491 ± 1.181% for Pool 2 (Samples 4–6), and 54.553 ± 0.763% for Pool 3 (Samples 7–9), confirming the high reproducibility and stability of the extraction method prior to pooling for biochemical characterization. The detailed mass balances, including the individual dry weights, net lyophilized extracts, remaining dry pellets, and processing losses are comprehensively summarized in Table 2.

Table 2. Comprehensive mass balances, residual fractions, and final extraction yield of lyophilized red pomegranate peel aqueous extract (R3PAE) across all nine samples.

Experimental Pool/Sample ID	Initial Dry Peel Mass (g)	Lyophilized Extract Net Weight (g)	Extraction Yield (%)	Residual Dry Pellet (g)	Processing Mass Loss (g)
Pool 1 Mean ± SD	1.005 ± 0.004	0.552 ± 0.026	55.176 ± 2.623	0.333 ± 0.006	0.120 ± 0.030
Pool 2 Mean ± SD	1.004 ± 0.002	0.550 ± 0.012	54.491 ± 1.181	0.290 ± 0.052	0.169 ± 0.062
Pool 3 Mean ± SD	1.005 ± 0.001	0.548 ± 0.008	54.553 ± 0.763	0.319 ± 0.006	0.138 ± 0.007
Mean (All Samples)	**1.004 ± 0.001**	**0.548 ± 0.016**	**54.742 ± 1.527**	**0.314 ± 0.035**	**0.142 ± 0.043**

Values are expressed as direct experimental measurements and mean ± standard deviation (SD).

The high solute recovery could be directly attributable to the optimization of the sequential processing parameters. Moreover, operating at 45 °C successfully decreased solvent viscosity and boosted capillary penetration [46,47] without crossing the critical thermal threshold that induces the oxidation or degradation of highly thermolabile compounds [47,48]. The mass balance analysis highlights the necessity of the triple cycle sequential approach [49,50].

As reported in Table 2, the process left an average insoluble residual dry pellet of 0.314 ± 0.035 g, while experiencing a minor, predictable processing mass loss (mean of 0.142 ± 0.043 g). This minimal loss could be linked to physical retention during the sequential liquid transfers, mechanical adhesion to the filter papers, and splattering during the final 15 min centrifugation at 4000× *g*. The resulting slow hygroscopic powder exhibited good stability when stored at −20 °C.

3.3. Biochemical Evaluation of the Total Polyphenolic (TPC), Flavonoid (TFC) and Anthocyanin Contents and the Related Antioxidant Activity (DPPH Assay)

Following the individual mass balance evaluation, the freeze-dried extracts were combined according to their original group assignment into three representative experimental pools (Pool 1: Samples 1–3; Pool 2: Samples 4–6; Pool 3: Samples 7–9). All subsequent biochemical evaluations (TPC, TFC, TAC, and DPPH assays) were conducted on these three consolidated pools in independent triplicates.

Total Polyphenolic Content (TPC)

Biochemical analysis revealed that the lyophilized red pomegranate peel pools aqueous extract (R3PAE) exhibits a high density of total phenolic content (TPC), quantified as a mean value of 62.1 ± 10 mg GAE eq./g DW, as reported in Figure 1 below. This considerable accumulation highlights the efficacy of the ultrasound assisted extraction protocol in disrupting the rigid cell wall matrix of the peel, thereby maximizing the release of secondary metabolites into the solvent.

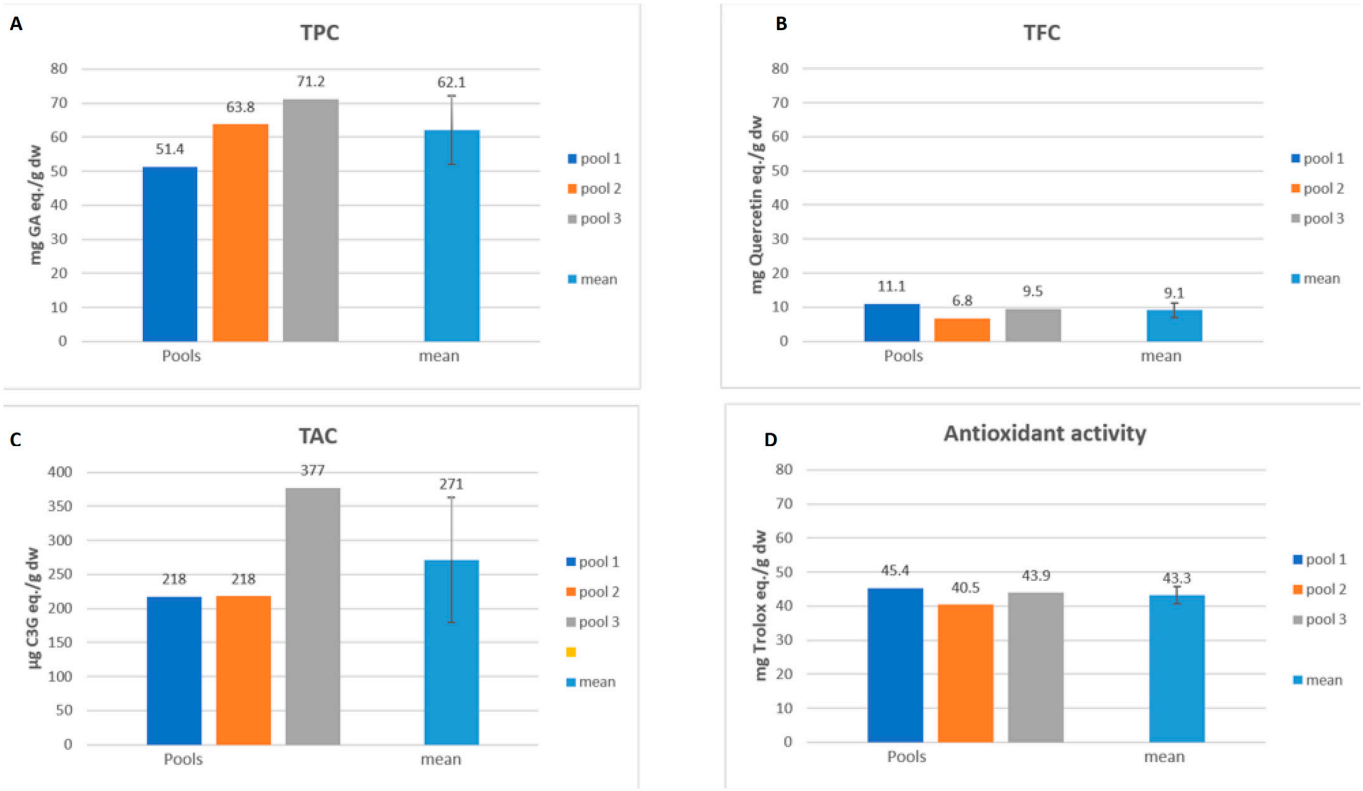


Figure 1. Biochemical profile and antioxidant capacity of the pomegranate peel extract across the three different experimental pools and their cumulative mean (± SD): (**A**) total phenolic content (TPC); (**B**) total flavonoid content (TFC); (**C**) total anthocyanin content (TAC); (**D**) free-radical scavenging activity determined via the DPPH assay.

To enable a direct comparison between our results, expressed on a dry weight basis, and the previous literature reporting data on a fresh weight basis for the same cultivar "Wonderful One" grown under identical pedoclimatic conditions [21], gravimetric conversion factors were derived. Based on our overall fresh peel dry yield of 39.41%, a mean conversion multiplier of 2.54 was calculated for our raw material. To account for the exact peel moisture content of 76.1% reported by Montefusco et al. (2021) [21] (corresponding to a dry matter content of 23.9%), a literature-specific conversion factor of 4.18 was applied. Multiplying the total phenolic content (TPC) value reported by Montefusco et al. (2021) [21] for fresh pomegranate exocarp of cv. Wonderful One (52.3 mg GAE/g FW) by this factor yields an equivalent dry weight benchmark of 218.8 mg GAE/g DW. The mean TPC value obtained for the lyophilized R3PAE extract in this study (62.1 ± 10 mg GAE/g DW) represents 28.4% of this total phenolic content.

This recovery rate is particularly notable considering that while analytical characterizations [21] utilize exhaustive organic solvent extractions to quantify total tissue accumulation, our process was performed exclusively in pure water via mild ultrasound assistance (UAE at 45 °C) without organic solvents. This could be associated with the capability of UAE to selectively isolate the most bio-accessible and highly water-soluble bioactive fraction (hy-

drolysable tannins) while preserving the high intrinsic biological and antioxidant potential of this agricultural byproduct.

Total Flavonoid Content (TPC)

In close correlation with the overall phenolic profile, the total flavonoid content (TFC) reached a mean value of 9.1 ± 2.2 mg QE eq./g DW, as reported in Figure 1 above. This specific class of low-molecular-weight metabolites accounts for approximately 14.7% of the total extracted polyphenolic pool, representing a primary functional fraction. When contextualized against the reference profile for cv. Wonderful One peels reported by Montefusco et al. (2021) [21] (4.7 mg CE/g FW, corresponding to 19.7 mg CE/g DW), our eco-friendly aqueous extract recovers approximately half of the total flavonoid pool intrinsic to the raw tissue.

The prominent presence of flavonoids in the R3PAE matrix serves as a crucial indicator of its bioactivity, as these molecules are widely recognized for their potent free-radical scavenging capacities, antimicrobial properties, and ability to form stable complexes within polymeric matrices. The quantitative stability of this fraction demonstrates that the subsequent lyophilization phase efficiently removed water via sublimation without inducing structural or chemical alterations in the thermolabile constituents of the extract.

Total Anthocyanin Content (TAC)

Regarding the pigment fraction, the quantitative analysis of total anthocyanins (TAC) exhibited a mean value of 271 ± 9 µg C3G eq/g DW. The determination of this water-soluble vacuolar anthocyanin is essential to delineate the exact biochemical profile of the studied cultivar.

In the fresh exocarp of cv. Wonderful One, Montefusco et al. (2021) [21] reported a TAC value of 104.8 µg CGE/g FW (equivalent to 438.5 µg CGE/g DW), dominated by cyanidin derivatives. The recovery of 271 µg C3G eq/g DW in our aqueous pool underscores that mild thermal-ultrasonic treatment efficiently leaches these polar pigments without accelerating their pH- or temperature-induced degradation.

Anthocyanins, which are notably abundant in the peel of mature red pomegranates, exhibit high susceptibility to pH fluctuations and environmental degradative factors. Consequently, these precise quantitative values not only estimate their specific contribution to the overall antioxidant activity of the complex but also predict the colorimetric impact and long-term stability of the extracts (R3PAE) when applied as functional additives or active agents in bio-packaging systems.

Evaluation of the Antioxidant Activity (DPPH Assay)

To comprehensively evaluate the biological efficacy of the recovered complex, the free-radical scavenging capacity of the extract was verified using the DPPH assay, yielding a final cumulative mean antioxidant activity of 43.3 ± 2.5 mg TE eq/g DW, as reported in Figure 1. This radical scavenging performance is directly driven by the robust concentrations of total phenolics and flavonoids quantified in the matrix, confirming that these secondary metabolites retain their donating capacity post lyophilization.

This aligns with the findings of Montefusco et al. (2021) [21], who demonstrated a strong linear correlation between total soluble phenolic content, hydrophilic antioxidant activity, and radical neutralizing capacity in pomegranate peels.

When evaluating the individual extraction stages, the antioxidant capacity showed excellent consistency across the distinct batches. This uniform distribution underscores the high reproducibility of the ultrasound-assisted extraction process, ensuring the free hydroxyl groups constituents responsible for mitigating oxidative stress are steadily and efficiently recovered. The strong capacity of the R3PAE matrix to neutralize stable free radicals highlights its exceptional potential as a functional, health-promoting substitute for synthetic antioxidants in active food packaging and other applications.

The substantial concentration of bioactive molecules in the R3PAE extract is directly linked to the removal of the native 60.59% water fraction during controlled low-temperature drying (45 °C). This dehydration process preserved thermal-sensitive constituents, including flavonoids and anthocyanins, which are key contributors to radical scavenging activity. This concentrated matrix is particularly advantageous for active packaging applications, as it provides high functional efficacy at lower biopolymer loading rates.

Preliminary Chromatographic Fingerprinting by UHPLC-DAD

The qualitative screening of the lyophilized aqueous pomegranate peel extract (R3PAE) via UHPLC-DAD at 280 nm provided a highly resolved chemical fingerprint, mapping the structural complexity of the recovered complex without the immediate need for exhaustive individual isolation. The selection of 280 nm as the monitoring wavelength is particularly suitable for polyphenolic screening, as it corresponds to the characteristic UV absorption maximum of the aromatic rings in hydroxybenzoic and hydroxycinnamic acid derivatives, as well as core hydrolysable tannin fragments [51,52]. By comparing the retention behavior, relative elution sequence, and UV-absorbance profiles of the main eluted peaks with established literature data for *Punica granatum* L. agricultural byproducts, a preliminary assignment of the major bioactive constituents was successfully achieved. Specifically, the chromatographic architecture demonstrated strong alignment and qualitative correlation with the standard HPLC profiles documented by El-Hamamsy & El-Khamissi (2020) [20], who thoroughly mapped the phenolic fractions of pomegranate peel extracts under highly compatible wavelength parameters (280 nm).

Major polyphenolic compounds were putatively assigned by matching UHPLC-DAD retention sequences and UV–Vis spectral curves with the published literature [20]. Without authentic reference standards or LC-MS/MS structural confirmation, these identifications remain putative and were intentionally restricted to qualitative chromatographic fingerprinting rather than absolute quantification. This non-targeted screening approach is widely recognized in natural product chemistry to confirm extract authenticity, batch-to-batch consistency, and overall compositional complexity prior to functional evaluation [53].

Based on this comparative fingerprinting analysis, the primary peaks resolved within the R3PAE matrix, as shown in Figure 2, can be putatively assigned to protocatechuic acid, syringic acid, ellagic acid, and iso-ferulic acid. These identified compounds represent key subclasses of pomegranate polyphenols, encompassing hydroxybenzoic acids (protocatechuic and syringic acids), hydroxycinnamic acids (iso-ferulic acid), and polyphenolic lactones (ellagic acid). The high DPPH radical scavenging capacity observed for R3PAE can be directly contextualized by the presence of these specific phenolic moieties.

The detection of this specific profile is highly consistent with the aqueous extraction pathways of pomegranate peel. Prior investigations have established that hydrothermal and acoustic cavitation treatments (UAE at 45 °C) efficiently cleave complex macromolecular matrices, liberating bound phenolic monomers into the aqueous phase [54]. Furthermore, the prominent peak referable to free ellagic acid reflects the successful mass transfer resulting from the cavitation-induced partial hydrolysis of larger hydrolysable tannins naturally abundant in pomegranate peels [52,55]. The retention and structural preservation of these target polyphenols underscore the non-destructive nature of the ultrasound-assisted extraction, confirming that R3PAE operates as a multi-component bioactive complex responsible for the observed DPPH antioxidant performance.

3.4. Minimum Inhibitory Concentration (MIC) by Resazurin Colorimetric Assay

The colorimetric broth microdilution assay, adapted from the resazurin reduction protocol optimized by Elshikh et al. (2016) [35], successfully established the antimicrobial profile of the lyophilized R3PAE across a two-fold serial dilution series ranging from 20 to

0.625 mg/mL. The metabolic shift of resazurin from its blue, non-fluorescent oxidized state to the pink, fluorescent resorufin served as a clear visual indicator of cell viability. During minimum inhibitory concentration (MIC) testing via the resazurin microdilution assay, high concentrations of the extract 20 mg/mL induced an immediate background chromatic shift due to the intense intrinsic pigmentation and high optical density of the crude polyphenols. To confirm that this spectral shift did not represent enzymatic dye reduction driven by viable microbial metabolism (conversion of non-fluorescent resazurin to pink resorufin), an independent dual-wavelength spectrophotometric verification was conducted at 570 nm and 600 nm [56,57]. By subtracting background absorbance of extract-only control wells at these specific wavelengths, true microbial metabolic inhibition was distinguished from optical interference caused by the dark extract matrix, preventing false-positive or false-negative MIC readings [58].

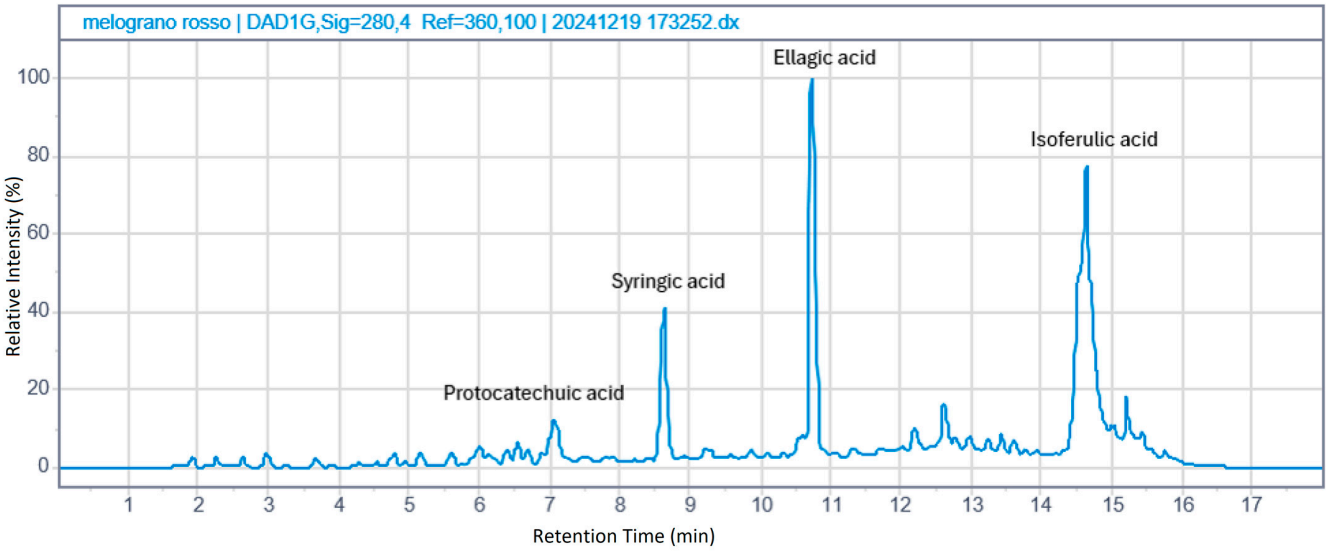


Figure 2. Preliminary chromatographic fingerprinting by UHPLC-DAD of the R3PAE.

The extract demonstrated a broad-spectrum minimum inhibitory concentration profile (Table 3), though susceptibility varied distinctly between Gram-positive and Gram-negative targets: *Bacillus subtilis* (MTCC 5376) exhibited a definitive MIC range of 2.5 to 5 mg/mL, verifying the high potency of the complex against spore-forming targets. Similarly, *Staphylococcus aureus* (ATCC 25923) displayed a high susceptibility, with a stabilized MIC fixed at 2.5 mg/mL, where the resazurin indicator remained strictly blue, signifying complete growth arrest.

Table 3. Minimum inhibitory concentration (MIC) values of R3PAE against bacterial strains.

Bacterial Strain	Observed MIC (mg/mL)
Staphylococcus aureus (ATCC 25923)	2.5
Bacillus subtilis (MTCC 5376)	2.5–5
Escherichia coli (ATCC 25922)	5
Pseudomonas aeruginosa (PA-01)	10

Values are expressed in mg/mL and represent analytical triplicates ($n = 3$) within a tested concentration range of 0.625 to 20 mg/mL.

Between Gram-negative bacteria, as anticipated, these strains required higher concentrations to achieve full inhibition. *Escherichia coli* (ATCC 25922) yielded an MIC value of

5 mg/mL, while the notoriously opportunistic and resistant *Pseudomonas aeruginosa* (PA-01) was successfully inhibited at an MIC of 10 mg/mL.

This observed susceptibility gradient, where Gram-positive strains are inhibited at lower concentrations than Gram-negative strains, directly aligns with the structural variations of the bacterial cell envelopes [59]. Gram-negative bacteria possess a rigid, asymmetric outer lipopolysaccharide membrane that acts as a selective permeability barrier, restricting the influx of hydrophobic and large hydrophilic molecules [59,60].

The pronounced antimicrobial capacity of R3PAE at these concentration thresholds can be attributed to the synergistic action of its unique polyphenolic fingerprint, specifically the probably rich presence of ellagic acid, protocatechuic acid, and specialized flavonoids determined in our chromatographic screening [20]. These bioactive molecules are known to disrupt bacterial homeostasis by permeabilizing the cytoplasmic membrane, cross-linking cell wall surface proteins, and inducing intracellular oxidative stress [61,62]. The absolute validity of the trial was confirmed by the controls, where the growth medium (negative control) induced an immediate, uniform shift to pink, while the gentamicin standard (positive control) maintained an unaltered blue profile across all inoculated wells.

3.5. Agar Disc Diffusion Screening for Bioactive Film Loading Determination

The preliminary antimicrobial screening of the R3PAE extract via the agar disc diffusion assay demonstrated a clear dose-dependent inhibitory effect against the tested bacterial panel [63,64]. This screening served as a foundational step to establish the minimum effective dose required to guide the rational loading and surface density design of the subsequent active biopolymer films.

The susceptibility profile mirrored the trends observed in the broth microdilution assays, with Gram-positive strains exhibiting significantly higher sensitivity to the extract compared to Gram-negative targets: *Bacillus subtilis* (MTCC 5376) demonstrated a highly sensitive threshold, initiating a clear visible zone of inhibition of 9 ± 1 mm at a low extract content of 0.5 mg/disc. Below this threshold (0.25 mg/disc), no inhibitory halo was resolved (6 mm). As the extract concentration escalated to 10 mg/disc, the inhibition zone for *B. subtilis* expanded progressively to 22 ± 2 mm. *Staphylococcus aureus* (ATCC 25923) displayed a closely matched susceptibility behavior, triggering an active zone of 8 ± 1 mm at 0.5 mg/disc and reaching a maximum halo of 21 ± 1 mm at the highest tested dose. These findings directly align with previous studies reporting high sensitivity of Gram-positive strains to aqueous pomegranate peel extracts rich in water-soluble polyphenols [23,65,66].

In contrast, between tested Gram-negative bacteria, both *Escherichia coli* (ATCC 25922) and *Pseudomonas aeruginosa* (PA-01) required a higher critical mass of bioactive compounds to overcome their outer membrane defenses [67]. *E. coli* remained completely unaffected at doses below 1 mg/disc, showing its first measurable inhibition zone (8 ± 1 mm) at 1 mg/disc. The highly defensive *P. aeruginosa* strain proved to be the most resilient, showing complete overgrowth up to 1 mg/disc and establishing a distinct zone of inhibition (8 ± 1 mm) only when reaching a threshold of 2.5 mg/disc (Table 4). This behavior is consistent with the literature indicating that higher concentrations of pomegranate peel polyphenols are necessary to penetrate the asymmetric outer membrane barrier of Gram-negative pathogens [68–70].

The amount of R3PAE to be incorporated into the film matrix was calculated by normalizing the inhibitory effect observed per cm^2. This concentration was derived from the ratio between the minimum effective dose determined on the disc and the surface area of the subsequent film casting. This area proportional calculation ensured that the final bioactive films would possess a theoretical antimicrobial surface density equivalent or higher to the effective minimum inhibitory thresholds observed during the disc diffusion screening.

Table 4. Inhibition zone diameters (mm) of target bacterial strains exposed to a concentration gradient of R3PAE extract for active film loading optimization.

Treated Dose/Control	*Bacillus subtilis* (MTCC 5376)	*Staphylococcus aureus* (ATCC 25923)	*Escherichia coli* (ATCC 25922)	*Pseudomonas aeruginosa* (PA-01)
0.25 mg/film	No inhibition	No inhibition	No inhibition	No inhibition
0.5 mg/film	9 ± 1	8 ± 1	No inhibition	No inhibition
1 mg/film	12 ± 1	11 ± 1	8 ± 1	No inhibition
2.5 mg/film	15 ± 1	14 ± 1	11 ± 1	8 ± 1
5 mg/film	18 ± 1	17 ± 1	14 ± 1	10 ± 1
10 mg/film	22 ± 2	21 ± 1	17 ± 2	13 ± 1
Negative Control (Solvent)	No inhibition	No inhibition	No inhibition	No inhibition
Positive Control (Gentamicin)	26 ± 1	25 ± 1	23 ± 2	21 ± 1

Target bacterial strain	Determined min. effective dose
***Staphylococcus aureus* (ATCC 25923)**	0.5 mg/film
***Bacillus subtilis* (MTCC 5376)**	0.5 mg/film
***Escherichia coli* (ATCC 25922)**	1 mg/film
***Pseudomonas aeruginosa* (PA-01)**	2.5 mg/film

All millimeter values are expressed as whole (mean ± SD) derived from three independent experiments, each conducted with three replicates. "No inhibition" signifies a complete absence of an inhibition zone.

To translate these discrete disc values into a scalable parameter for active packaging development, the minimum effective dose observed on the paper discs was normalized against the surface area of the disc [71]. Given that the paper discs possess a standard diameter of 6 mm, their surface area A_{disc} is calculated using the standard formula:

$$A_{disc} = A = \pi \times r^2 = \pi \times (0.3\ cm)^2 = 0.283\ cm^2$$

Since *B. subtilis* and *S. aureus* displayed initial vulnerability at 0.5 mg/disc, the minimum effective surface density S_{eff} required to induce a localized antimicrobial effect was determined as follows:

$$S_{eff} = \text{Minimum effective dose}/A_{disc} = 0.5\ mg/0.283\ cm^2 = 1.77\ mg/cm^2$$

Conversely, target Gram-negative strains required higher baseline loadings: *E. coli* (1.0 mg/disc) translated to an effective theoretical surface density of 3.53 mg/cm^2, whereas *P. aeruginosa* (2.5 mg/disc) strictly demanded a considerably higher payload of 8.83 mg/cm^2 to trigger initial inhibition. Although this theoretical value guarantees antimicrobial pressure against highly resilient pathogens, incorporating higher extract densities into the biopolymer formulation severely compromise the structural integrity, flexibility, and morphological uniformity of the cast films. Consequently, 3.53 mg/cm^2 was selected as the upper feasibility limit for active film development, prioritizing Gram-positive targets and *E. coli* while maintaining matrix mechanical stability.

This mathematical extrapolation guarantees that the final cast macromolecular films will maintain a theoretical surface density high enough to exert sustained antimicrobial pressure when applied directly to food or biomaterial surface [2,6].

3.6. Preparation of Bioactive Films

Following the protocol described by Martins et al. (2012) [14], a 60/40 ratio of locust bean gum to kappa-carrageenan was selected for the formulation of the polymeric matrix. However, slight modifications were made, specifically adjusting the glycerol to 0.75% (*w*/*v*). This optimization was necessary as the starting commercial raw materials used in this study (E410 carob seed flour and E407 k-carrageenan) differed significantly from the pure/refined biopolymers described in the reference literature. Specifically, E410 and E407 contain intrinsic food-grade co-constituents, including proteins (slightly below 7% in E410), salt and sugars (10% and <28% respectively in E407), which actively influence the macromolecular entanglement, solution viscosity, and physical gelation of the film-forming matrix.

Preliminary solvent casting trials confirmed the excellent synergy between LBG and k-car in film formation. In line with literature findings for pure hydrocolloid-based films, the inclusion of glycerol proved fundamental to overcoming the intrinsic structural brittleness of the polymer chains, ensuring the flexibility, continuity, and handling properties necessary for the film [16,72].

The incorporation of freeze-dried R3PAE at a controlled temperature of 40 °C represented a critical choice for the success of the active formulation. Maintaining the casting solution at 40 °C also restricted premature thermal cross-linking or polyphenol aggregation, favoring smooth macromolecular entrapment upon solvent evaporation. This specific thermal window allowed for the preservation of the integrity of the thermosensitive bioactive compounds within the extract [73,74]. Visually, both the control and active films appeared as homogeneous, continuous structures, free of fractures or macroscopic porosity after dehydration in a climate chamber.

While the control film exhibited remarkable transparency and a clear appearance (Figure 3A), the introduction of the R3PAE extract imparted a slight yellow/orange coloration to the active matrix without altering surface uniformity (Figure 3B). This characteristic chromatic shift toward yellow/orange hues is directly associated with the light-absorption properties of chromophoric polyphenolic structures, such as ellagitannins and flavonoids, naturally present in pomegranate peel. This also suggests excellent compatibility and a homogeneous distribution of the bioactive components within the three-dimensional network formed by LBG and k-car, similarly to observations in previous studies on the incorporation of natural extracts and plasticizers into plant gum-based edible films, where proper intermolecular interaction promoted the formation of uniform and smooth structures [75,76]. The absence of phase separation or domain segregation further confirms that extensive intermolecular hydrogen bonding occurred between the hydroxyl groups of the polyphenols and the hydrophilic backbone of the LBG/k-car hydrocolloids.

3.7. Antimicrobial Efficacy of the Developed Bioactive Film

The antimicrobial efficacy of the R3PAE-loaded films was evaluated using the agar diffusion method, ensuring intimate and uniform contact between the polymer matrix and the culture medium [36,63,64]. This assay provided a direct assessment of the active films' capacity to successfully release the entrapped antimicrobial agents into the surrounding medium and inhibit the growth of the tested pathogenic strains. The results revealed a significant enhancement of the inhibitory efficacy compared to the preliminary paper disc screening, suggesting optimized release kinetics or potential synergistic bioactivity effects between the film polymers and the extract [2,6,71]. As presented in Table 5, square film specimens (5 mm × 5 mm, 0.25 cm^2) exhibited distinct inhibition zones against the target microorganisms. Specifically, total inhibition diameters of 8 ± 1 mm and 9 ± 1 mm were observed for *P. aeruginosa* and *E. coli*, respectively, and 13 ± 2 mm and 15 ± 1 mm were

observed for *S. aureus* and *B. subtilis*, confirming the successful release and activity of the R3PAE extract from the film matrix.



Figure 3. Macroscopic appearance and visual comparison of the prepared polymeric films. Visual appearance and structural morphology of the developed biopolymer formulations: (**A**) control film formulated with a 60/40 ratio of locust bean gum (LBG) to kappa-carrageenan (k-car) and 0.75% (*w*/*v*) glycerol, displaying high transparency and a clear appearance; (**B**) active film incorporated with freeze-dried R3PAE extract, exhibiting a characteristic slight yellow/orange coloration. All matrices show a homogeneous, continuous structure free of fractures or macroscopic porosity, indicating excellent compatibility and uniform distribution of the bioactive components.

Table 5. Inhibition zone diameters (mm) of target bacterial strains exposed to the bio-active film (surface density: 3 mg/cm^2).

Target Bacterial Strain	Control Film (Unloaded)	Bioactive Film (3 mg/cm^2)
***Bacillus subtilis* (MTCC 5376)**	No inhibition	15 ± 1
***Staphylococcus aureus* (ATCC 25923)**	No inhibition	13 ± 2
***Escherichia coli* (ATCC 25922)**	No inhibition	9 ± 1
***Pseudomonas aeruginosa* (PA-01)**	No inhibition	8 ± 1

Values are expressed as mean ± standard deviation derived from three experiments with three independent replicates ($n = 3$). The reported inhibition zone corresponds to the total diameter, including the 5 mm × 5 mm square film specimen (0.25 cm^2). "No inhibition" represents the complete absence of an inhibition zone around the square film. Control films were tested on the same plates to assess any baseline inhibitory effects from the polymer matrix itself.

As expected, control films prepared without the R3PAE extract generated no inhibition zone around the polymer margins, confirming that the hydrocolloid matrix acts strictly as an inert, biocompatible carrier system and that the observed antibacterial effects stem entirely from the release kinetics of the loaded extract [18,44,76]. Conversely, gentamicin disc used as a positive control yielded pronounced inhibition zones against all tested strains, thereby validating the reliability of the assay conditions and confirming the baseline susceptibility of the indicator microorganisms.

Mirroring the susceptibility trends of the preliminary assay, Gram-positive strains exhibited the highest sensitivity, driven by the absence of an outer membrane hindering polyphenolic penetration [62,77]. However, the magnitude of the inhibition was markedly superior: *Bacillus subtilis* generated an extensive inhibition zone of 15 ± 1 mm. This outcome

is particularly noteworthy when compared to the 9 ± 1 mm recorded in the disc diffusion assay at an equivalent applied mass. *Staphylococcus aureus* followed a closely matched susceptibility behavior, displaying strong inhibition with 13 ± 2 mm. This demonstrates the excellent capacity of the solid matrix to properly hydrate and facilitate the diffusion of the active compounds into the agar. Unlike inert cellulosic paper discs, which often restrict the release of large polyphenolic molecules due to internal steric hindrance or physical adsorption, the swelling capability of the hydrophilic LBG/k-carrageenan network upon contact with agar moisture expands the biopolymer mesh, thereby accelerating the mass transport of water-soluble polyphenols into the gel medium [14,16].

Following the theoretical screening range estimated between 1.77 mg/cm^2 and 3.53 mg/cm^2, a series of exploratory film formulations were tested starting from a baseline of 1.77 mg/cm^2 upwards. While preliminary variations partially affected *Escherichia coli* (generating a measurable halo of 9 ± 1 mm), achieving consistent and reliable inhibition against the highly resilient *Pseudomonas aeruginosa* required further optimization due to the restrictive lipopolysaccharide barrier characteristic of Gram-negative bacteria [59,67,78].

As predicted by the theoretical extrapolation, lower active loadings proved insufficient to inhibit *P. aeruginosa*. To overcome this recalcitrance and breach the restrictive outer membrane barrier, the active content was increased to a surface density of 3 mg/cm^2, which was selected as the optimal formulation, successfully yielding an inhibition halo of 8 ± 1 mm [22,23,69]. However, attempting to increase the active loading beyond this threshold introduced a clear material trade-off: the physical performance of the film deteriorated significantly, evidenced by a noticeable reduction in mechanical strength (increased brittleness and reduced tensile properties) alongside an excessively dark, over-saturated coloration. These observations demonstrate that while theoretical extrapolation accurately dictates the bio-efficacy threshold, practical film formulation must negotiate a careful balance between antimicrobial potency against resilient Gram-negative strains and optimal physicochemical properties. The decline in mechanical performance observed at higher active concentrations required for *P. aeruginosa* inhibition can be attributed to the disruption of the polymeric network structure, leading to stress concentration points and reduced film flexibility. Furthermore, increasing the active loading to satisfy the theoretical threshold for *P. aeruginosa* resulted in a marked decrease in film transparency and an intense color saturation, which may restrict the aesthetic appeal for transparent packaging applications.

As already indicated, this favorable outcome can be explained by the excellent diffusion dynamics and mass transfer provided by the LBG/k-carrageenan blend, which optimize the release of the bioactive compounds and allow the film to effectively inhibit even highly resilient Gram-negative strains [14,72]. Reaching an effective inhibitory halo against *P. aeruginosa* at 3 mg/cm^2 highlights the practical potential of this film as an active packaging material. In real food systems (such as cold cuts, fresh meat or seafood), maintaining a continuous threshold concentration of active phenolics at the food-package interface is critical to suppressing volatile nitrogen compound formation and delaying surface microbial spoilage during refrigerated storage.

3.8. Structural Polymer Evaluation via FTIR-ATR

To elucidate the structural alterations and intermolecular chemical interactions resulting from the incorporation of R3PAE and the non-polymeric native co-constituents into the biopolymer matrix, FTIR-ATR analysis was conducted (Figure 4). The representative spectrum successfully displays the characteristic absorption bands corresponding to the polysaccharide backbone. As shown in the Figure 4, a broad and intense band is observed in the 3600–3100 cm^{-1} region, which is typically assigned to the stretching vibrations of the hydroxyl (-OH) groups commonly involved in intra- and intermolecular hydrogen

bonding. The peaks detected around 2900 cm^{-1} correspond to the C-H stretching vibrations of aliphatic chains. Crucially, the specific composition of the hydrocolloid matrix is confirmed by the distinct absorption bands resolved in the fingerprint region (1250–650 cm^{-1}), highlighted in the magnified inset of Figure 4. These include the S=O stretching vibration of sulfate ester groups at approximately 1200 cm^{-1}, C4-O-S stretching at 840 cm^{-1}, and C-O-C stretching at 930 cm^{-1}, alongside robust C-O, C-O-C, and C-O-H stretching vibrations between 1000 and 1150 cm^{-1} [14–16].

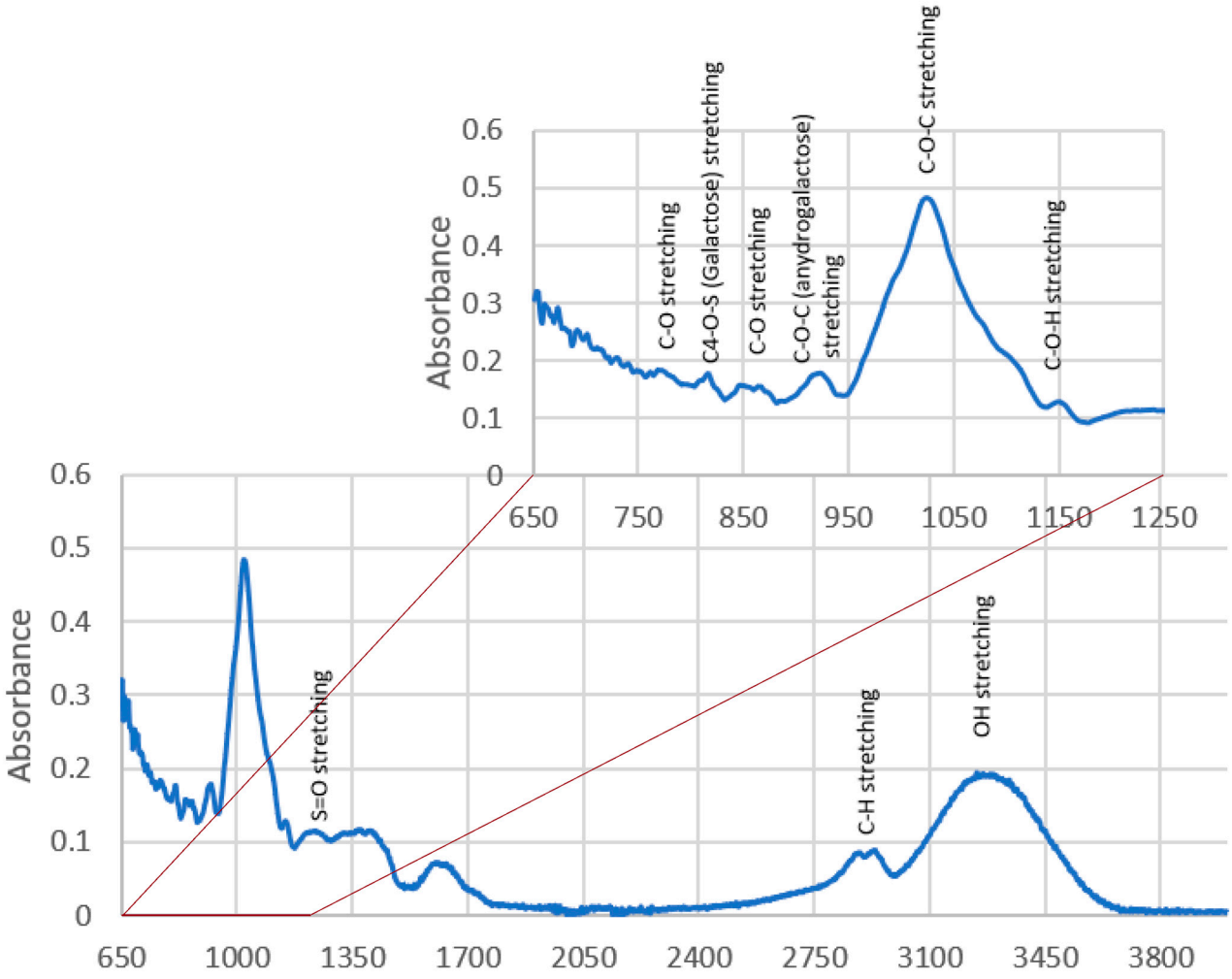


Figure 4. FTIR-ATR spectrum of the active edible film matrix. FTIR-ATR spectrum of the active edible film matrix over the 4000–650 cm^{-1} spectral range. The inset provides a magnified view of the fingerprint region (1250–650 cm^{-1}, highlighted by the red lines), identifying the characteristic functional groups of the polysaccharide backbone.

In this context, emphasis was placed on evaluating potential shifts and intensity variations connected with the possible formation of intermolecular hydrogen bonding networks, which are crucial for tailoring the structural and functional properties of active edible films.

The incorporation of food-grade E410 and E407 matrices, introducing native protein, salt and sugar fractions, alongside R3PAE polyphenols, resulted in FTIR-ATR profiles that fully overlapped with the control film. These native non-polymeric co-constituents and polyphenolic compounds integrate into the polysaccharide matrix through non-covalent physical interactions (such as hydrogen bonding, hydrophobic interactions, and physical entanglement within free volume spaces) without generating new covalent linkages or altering the primary polymer backbone [79,80].

The absence of pronounced spectral peak shifts or newly emerging absorption bands in the FTIR-ATR spectra of active films relative to the control film does not contradict the occurrence of polyphenol–matrix interactions. Phenolics typically incorporate into biopolymer networks through these non-covalent mechanisms, which leave the primary chemical structure undisturbed. Furthermore, the broad, intense absorption bands inherent to the carbohydrate matrix frequently mask subtle frequency shifts induced by low polyphenol concentrations [81]. Rather than forming chemical cross-links, the incorporated polyphenols act as physical fillers occupying free volume within the matrix, stabilizing the hydrocolloid network through physical entanglements and weak electrostatic associations without altering the primary FTIR vibrational signatures.

This absence of spectral differentiation indicates that the functional groups of the polyphenolic compounds overlap within the prominent absorption bands of the polysaccharide hydrocolloids (specifically the broad -OH and carbohydrate C-O) or are loaded at a ratio fully accommodated within the matrix free volume. Consequently, the active extract was integrated without altering the primary chemical structure or disrupting the fundamental covalent bonds of the polymer backbone [44,76]. The preservation of this baseline spectroscopic profile indicates that the blended network of kappa-carrageenan and locust bean gum establishes a highly stable, dominant, and robust structural framework [14,16]. At a macroscopic level, the fact that this primary polysaccharide–polysaccharide framework remains completely undisturbed ensures that the material maintains its optimal functional performance. This structural preservation correlates directly with the film's functional behavior; preserving the synergistic junction zones between the double helices of kappa-carrageenan and the unsubstituted mannose regions of LBG maintains high mechanical tensile strength (TS) and limits matrix free volume, which in turn supports low Water Vapor Permeability (WVP) [6,14,75]. Ultimately, the overlapping FTIR profile validates that the incorporation of the active extract successfully yields a structurally intact, highly functional biopolymer matrix suitable for active food packaging applications. Therefore, any contribution of polyphenol–polysaccharide interactions to the mechanical and barrier properties discussed in the following sections should be regarded as a plausible but indirect interpretation rather than direct spectroscopic evidence.

3.9. Film Thickness and Moisture Content

The physical characterization of the developed matrices revealed a mean thickness of 19 ± 2 µm for the control film, which slightly increased to 21.7 ± 1 µm upon the incorporation of R3PAE. This slight thickness increment is conventionally attributed to the higher total solids content in the casting solution, structural reorganization of the biopolymer network, and the physical entrapment of the active polyphenolic compounds within the interstitial spaces of the polymer matrix [14,82–84].

Regarding the gravimetric evaluation, both control and bioactivated film formulations exhibited a constant moisture content of approximately 23.6 ± 0.8%. This indicates that the addition of the polyphenolic extract did not drastically alter the intrinsic water retention capacity or the drying behavior of the hydrocolloid matrix. Instead, the hydration properties were predominantly governed by the polysaccharide ratio (k-carrageenan/LBG) and the plasticizer concentration [14,84].

Interestingly, the equilibrium moisture content observed in this study (23.6 ± 0.8%) for the 60/40 LBG/k-carrageenan matrix represents a noticeable increase compared to the value of 21.08 ± 1.13% reported by Martins et al. (2012) [14] for a similar hydrocolloid blend (40/60 k-carrageenan/LBG). This discrepancy may be mainly attributed to differences in plasticizer loading and biopolymer ratio. In the current formulation, glycerol was added at 75% *w*/*w* based on total dry polymer weight, whereas a lower concentration (30% *w*/*w*) was

utilized by Martins et al. (2012) [14]. Glycerol acts as a small, highly hygroscopic polyol that embeds between adjacent polysaccharide chains, disrupting inter-chain hydrogen bonds, expanding matrix free volume, and exposing hydroxyl groups that establish an extensive hydrogen-bonding network to bind water molecules [85–87].

Additionally, the modified biopolymer ratio of 60/40 *w*/*w* LBG/k-carrageenan increases the proportion of non-gelling galactomannan chains compared to the 40/60 *w*/*w* ratio in Martins et al. (2012) [14]. The steric hindrance imposed by LBG's galactose side-branches inhibits dense helicoidal junction zone formation between k-carrageenan double helices, yielding a looser, less crystalline matrix. This structural widening relaxes the polymer network, creating additional molecular cavities capable of entrapping a greater volume of interstitial moisture [14,75,87]. Consequently, the surplus of glycerol overrode the lower intrinsic hydrophilicity of the dominant LBG fraction, resulting in a more water-retentive, flexible, and cohesive film structure.

3.10. Mechanical Properties

The core mechanical parameters, maximum Force at Break, tensile strength (TS, MPa), and Elongation at Break (EB, %), of the neat control film (Ctrl-empty), the active biopackaging film incorporated with the red pomegranate peel aqueous extract (R3PAE), and a commercial packaging reference film (Ctrl-coop) were systematically evaluated and cross-examined with literature benchmarks.

The mechanical profiles derived from the raw experimental data revealed great performance for the developed formulations. The neat control film (Ctrl-empty), characterized by a thin cross-section of 19.2 µm, sustained a maximum breaking force of 484 ± 66 g, which mathematically yielded a high TS of 41.20 ± 5.62 MPa. Concurrently, the matrix exhibited a high flexibility, achieving a maximum elongation of 42 ± 3 mm, corresponding to an EB of 84.0 ± 6.0%. Remarkably, upon the incorporation of the bioactive red pomegranate peel extract (R3PAE; 21.7 µm thickness), a highly favorable structural reinforcement took place: the matrix withstood a maximum breaking force of 636 ± 13 g, resulting in a significantly elevated TS of 47.90 ± 0.98 MPa, while maintaining high elasticity (EB of 80.0 ± 2.0%).

These mechanical values represent a good behavior for carbohydrate-based packaging. In biopolymer physics, mechanical resistance and ductility are traditionally mutually exclusive, where structural strategies that amplify tensile strength routinely trigger severe matrix embrittlement. In our optimized formulations, the coexistence of a good TS (41–48 MPa) and a very high elongation (>80%) is directly attributed to the synergistic interaction between the k-car/LBG structural framework and the high glycerol plasticization protocol. From a macromolecular perspective, k-carrageenan undergoes a thermally reversible coil-to-helix transition upon cooling, assembling into rigid junction zones. The addition of LBG, a galactomannan with long unsubstituted mannan segments, enables cooperative intermolecular association between these smooth mannose regions and the carrageenan double helices. This synergistic junction prevents phase separation and forms a tight, cohesive structural framework capable of enduring high baseline mechanical stress (TS = 41.20 MPa) even prior to active compound loading [14–16]. The abundant plasticizer molecules effectively increase the free volume between the LBG macromolecular backbones and the k-car helical domains, guaranteeing high chain mobility. Generally, polyphenolic cross-linking restricts segmental chain mobility, leading to severe material embrittlement and a drastic drop in elongation. However, the developed formulation successfully preserved matrix ductility (EB = 80 ± 2%). This behavior is putatively governed by a dynamic balance between glycerol-mediated plasticization and polyphenol-mediated hydrogen bonding. Glycerol molecules intercalate between the polysaccharide backbones, increasing molecular mobility and providing a lubricative spacer effect. Simultaneously, the non-covalent nature of the

polyphenolic hydrogen bonds may allow them to reversibly dissociate and reform under mechanical deformation. This hypothesized dynamic bond exchange enables macromolecular sliding under uniaxial tension, dissipating mechanical energy while preventing catastrophic brittle failure [82].

The mechanical performance of the developed films exhibited very good values (TS = 41.20–47.90 MPa, EB = 80.0–84.0%), vastly outperforming literature benchmarks relying on pure biopolymers [14], reporting TS of 14.2 MPa and EB of 43.1% for 40/60 k-car/LBG. This remarkable enhancement is directly attributable to the use of commercial food-grade raw materials (E410 carob seed flour and E407 k-carrageenan) instead of highly purified polymers.

Within food-grade legal limits, E410 contains a native protein fraction of slightly less than 7%, whereas E407 comprises salt (10%) and sugars (<28%). These non-polymeric co-constituents play a decisive structural role: the native proteins (<7%) in E410 act as natural physical crosslinkers and structural fillers, establishing additional non-covalent hydrogen bonding and hydrophobic interactions with both galactomannan and sulfated galactan chains, thereby increasing tensile strength; the soluble sugars and salt in E407 act as dynamic co-plasticizers and domain fillers that occupy interstitial free volume.

In addition to the baseline structural contributions provided by the native protein, sugars and salt fractions, the observed performance suggests a probable polyphenolic-mediated structural reinforcement effect. The multi-hydroxyl active compounds inherent to the R3PAE extract are hypothesized to potentially form secondary intermolecular hydrogen bonds with the free functional groups of the polysaccharide backbones. The polyphenolic profile of R3PAE, characterized by high concentrations of hydrolyzable tannins, may play a decisive role in this matrix fortification. These molecules possess multiple phenolic hydroxyl groups that may potentially act as polyfunctional physical crosslinkers. These active sites are thought to form a network of non-covalent hydrogen bonds with both the anionic sulfate ester groups k-carrageenan and the hydroxyl moieties of LBG [18]. This proposed supramolecular cross-linking could increase the effective cross-link density of the network, potentially allowing incoming mechanical loads to be distributed over a higher number of non-covalent bonds and potentially requiring greater energy input to initiate matrix breakdown [76]. This proposed interconnection may have contributed to the observed reinforcement of the matrix without restricting its capacity to undergo massive elongation before reaching structural failure.

This hypothesis is further supported by the notable reduction in the standard deviation observed for the R3PAE formulation relative to the control, suggesting that the bioactive extract may have promoted a more homogeneous matrix organization, eliminating localized micro-structural discontinuities and distributing tensile stress evenly across the film plane. During the solvent evaporation stage of film casting, local density fluctuations typically create sub-micron voids that act as stress concentration sites, predisposing the material to premature and variable local rupture. Polyphenolic compounds penetrate these interstitial free volumes, acting as structural domain fillers that heal micro-structural discontinuities [84]. Consequently, applied uniaxial stress is dissipated uniformly across the film plane, resulting in high mechanical reproducibility and structural integrity.

However, it must be stressed that all this explanatory mechanism remains putative and probable at this stage. While this macro-mechanical optimization aligns with the integrity and stability of the primary polysaccharide framework demonstrated through FTIR-ATR analysis, baseline FTIR-ATR spectra alone cannot unequivocally confirm the specific spatial nature or precise density of these hydrogen bonds. Consequently, further in-depth FT-IR spectroscopic investigations along with additional advanced structural characterizations

will be performed in subsequent studies to further clarify these chemical interactions and how they could be associated with the underlying mechanical performance enhancement.

When compared to commercial and literature benchmarks, the developed active formulation establishes a good industrial advantage. The TS of the R3PAE film is more than double that of the used commercial reference film and significantly surpasses the landmark values reported by Martins et al. (2012) [14] for equivalent films (with pure polymers only). While the commercial control displayed a higher deformation capacity, the developed R3PAE successfully reconciles high mechanical toughness, structural density, and structural thinness.

3.11. Surface Hydrophobicity and Water Contact Angle (WCA)

The surface wettability and hydrophobicity of biopolymer films constitute pivotal parameters in food packaging development, directly influencing the material's behavior when in contact with moisture-rich food matrices and its stability under varying storage atmospheres. Surface hydrophobicity was quantitatively determined by measuring the static water contact angle (WCA), where values below 90° designate a hydrophilic surface profile, whereas angles exceeding 90° classify the material as hydrophobic [88,89].

The neat control film (Ctrl-empty) exhibited a remarkably high static WCA of 117° ± 3°, clearly demonstrating a hydrophobic surface profile. This hydrophobic behavior is highly interesting and unconventional for pure carbohydrate-based matrices, which are typically characterized by an abundance of exposed hydrophilic hydroxyl (-OH) groups along the macromolecular backbones of k-carrageenan (k-car) and locust bean gum (LBG) [14,16]. This distinct performance suggests that the specific solvent casting and climate-controlled drying parameters (45 °C and 15% RH) optimized in this study favored a highly dense, compact structural rearrangement [90]. This efficient molecular packing likely promoted the internal orientation of polar groups via intense intra- and intermolecular hydrogen bonding, leaving the more hydrophobic hydrocarbon segments exposed on the outer film topography [82].

Upon the incorporation of the red pomegranate peel aqueous extract (R3PAE), the static WCA significantly decreased to 105° ± 6°. This reduction in the contact angle indicates an enhanced surface affinity for water molecules, representing increased wettability compared to the control matrix. This phenomenon is directly ascribed to the massive influx of highly polar, water-soluble polyphenolic constituents inherent to the R3PAE extract [18,20]. These bioactive phytocompounds introduce an extensive network of peripheral, free hydroxyl groups that populate the outer film plane, actively engaging in hydrogen bonding with the deposited water droplet and accelerating its spreading at the solid–liquid interface [76].

Crucially, despite this controlled decrease in WCA, the active R3PAE firmly maintained its hydrophobic character, remaining well above the 90° threshold. This represents a significant technological advantage for active packaging applications, as the retention of surface hydrophobicity ensures optimal moisture resistance, preventing the film from prematurely dissolving or swelling when exposed to high-moisture food products [2,6].

Furthermore, the narrow standard deviations observed for both formulations demonstrate that the custom-tensioned solvent-cast matrices retained excellent topographic uniformity and structural equilibrium, effectively preventing uncontrolled localized curling during analysis [40]. This surface wetting behavior perfectly complements the outstanding mechanical performance previously discussed, confirming that the optimized blend successfully reconciles structural density, high tensile resistance, and a functional moisture-resistant interface.

3.12. Water Vapor Barrier Properties

The evaluation of water vapor barrier capacity is a primary quality index for active food packaging materials, as moisture migration directly governs critical degradative phenomena such as lipid oxidation, structural softening, and microbial proliferation in hydrophilic foods [82]. The active bio-packaging film incorporated with the red pomegranate peel extract (R3PAE) demonstrated a remarkably low Water Vapor Transmission Rate (WVTR) of 2 ± 0.15 g/m^2 × 24 h, which corresponds to a highly restricted Water Vapor Permeability (WVP) of $0.19 \pm 0.01 \times 10^{-11}$ g·m^{-1}·s^{-1}·Pa^{-1}. To put this result into perspective, standard polysaccharide-based active films documented in the recent state-of-the-art packaging literature routinely exhibit significantly higher transmission rates, typically ranging from 40 to well over 120 g/m^2 × 24 h under comparable testing conditions [91]. This historical limitation arises because the essential incorporation of hydrophilic plasticizers like glycerol conventionally opens up the macromolecular structure, creating preferential channels that facilitate rapid water molecule diffusion [92]. Achieving a barrier performance of merely 2 ± 0.15 g/m^2 × 24 h places the developed R3PAE active film in the elite tier of sustainable packaging materials, effectively bridging the performance gap between biopolymers and petroleum-derived synthetic plastics, closely matching the standard benchmarks of conventional low-density polyethylene [1,3].

This unprecedented moisture resistance is driven by two highly synergistic phenomena within the matrix: the synergistic presence of native protein (<7%), salt (10%) and sugar (<28%) fractions within the commercial E410 and E407 raw materials. Concurrently, native proteins, salt and sugars fill microscopic free volume voids and could engage exposed hydroxyl groups in strong hydrogen bonding networks, restricting water molecule mobility and effectively matching the moisture barrier performance of synthetic low-density polyethylene (LDPE); as supported by the mechanical reinforcement and high surface hydrophobicity of the matrix, the multi-hydroxyl phytocompounds inherent to the R3PAE extract may act as physical cross-linking agents [93]. The observed reduction in water vapor transmission may be associated with hydrogen-bond interactions between polyphenols and polysaccharides, which could decrease the accessibility of free hydroxyl groups to water molecules through the thin 21.7 μm film plane [94].

3.13. Oxygen Transmission Rate (O_2TR) and Permeability (O_2P)

Oxygen acts as the primary catalyst for numerous food spoilage mechanisms, including the rancidity of unsaturated fats, nutritional vitamin degradation, and the proliferation of aerobic molds. Consequently, maintaining a strict oxygen barrier is a fundamental prerequisite for long shelf-life. Evaluated under the dry testing conditions by the ASTM D3985 standard [43], the R3PAE active film exhibited a low Oxygen Transmission Rate O_2TR of 1.12 ± 0.08 cm^3/(m^2 × 24).

This good gas barrier performance provides further evidence of the high structural density engineered within the formulation. In polymer physics, carbohydrate-based matrices possess a natural advantage against non-polar gases due to their highly polar, tightly hydrogen-bonded crystalline networks that lack affinity for O_2. In the case of the R3PAE formulation, the encapsulated polyphenolic clusters may occupy part of the interstitial free volume of the biopolymer maze, acting as structural nanofillers that seal micro-cavities within the LBG/k-car framework. This spatial obstruction drastically lowers the gas diffusion coefficient, reducing the calculated Oxygen Permeability (O_2P) to a low value of $2.71 \pm 0.19 \times 10^{-19}$ cm^3·m·m^{-2}·s^{-1}·Pa^{-1}, offering protective performance for oxygen-sensitive food products.

The very low O_2TR and O_2P values observed for the R3PAE active film align well with recent advancements in the biopolymer packaging literature. Previous studies investigating

binary blends of k-carrageenan and locust bean gum (LBG) have demonstrated that the synergistic intermolecular interactions between the helical structures of k-carrageenan and the smooth regions of LBG create a tightly packed, dense crystalline network [13]. This compact macromolecular arrangement significantly restricts the free volume available for gas molecules to migrate, providing an inherent advantage over single-polymer films.

Furthermore, the integration of natural extracts and functional additives into polysaccharide matrices has been widely documented to exert a profound effect on barrier performance [12,83]. As indicated in recent food packaging evaluations by Lazić et al. (2020) [95], high-oxygen-barrier materials generally require O_2TR values within the strategic threshold of 0.1^{-30} cm^3 m^{-2} × 24 h, depending strictly on the oxygen sensitivity of the packaged food. The incorporation of well-dispersed functional components into biopolymeric structures introduces a tortuous diffusion path that lengthens the route required for gas molecules to permeate, thereby effectively diminishing overall oxygen transport across the matrix [95]. While excessive concentrations of hydrophilic plant extracts can occasionally disrupt polymer continuity, optimized formulations such as the R3PAE active film benefit from robust hydrogen bonding interactions and structural densification. These molecular interactions effectively immobilize polymer segments and plug microscopic interstitial cavities, successfully lowering both the diffusion and transmission rates of oxygen.

3.14. Carbon Dioxide Transmission Rate (CO_2TR) and Permeability (CO_2P)

The carbon dioxide barrier profile plays a decisive role in defining the internal gas composition and maintaining the modified atmosphere packaging (MAP) systems commonly used for fresh produce and protein preservation. The active R3PAE film showed a low CO_2 transmission rate to an optimized value of 4.65 ± 0.34 cm^3/m^2 × 24 h.

In agreement with polymer permeation laws, the transmission of CO_2 across polar matrices is traditionally higher than that of O_2 due to the high condensability and superior chemical solubility of carbon dioxide within hydrophilic networks, driven by its significant quadrupole moment interacting with the exposed polar zones of the polysaccharides. However, the capacity of the active R3PAE film to maintain a low CO_2 transmission rate demonstrates that the extensive hydrogen bonding network established between the extract and the biopolymer backbones may have partially counteracted this solubility advantage. By heavily compressing the matrix segments, the cross-linked framework successfully limited the micro-Brownian motions of the polymer chains, arresting the plasticization typically induced by gas dissolution and guaranteeing outstanding gas containment properties, yielding a balanced Carbon Dioxide Permeability CO_2P of 11.26 ± 0.78 × 10^{-19} $cm^3 \cdot m \cdot m^{-2} \cdot s^{-1} \cdot Pa^{-1}$.

When compared with broader literature data on biopolymer-based packaging, the CO_2TR value of the R3PAE film places the material in an exceptionally competitive performance tier. Neat, unplasticized or lightly modified polysaccharide films (such as pure starch, unmodified carrageenan, or chitosan matrices plasticized with high glycerol contents) routinely exhibit significantly higher CO_2 transmission rates, often ranging from 15 to over 50 cm^3/m^2 × 24 h due to the loose amorphous regions and wide interstitial free volumes that facilitate rapid gas diffusion [81,82,96]. Conversely, highly specialized nanocomposite or reinforced bio-films achieve lower CO_2TR values, sometimes falling below 1–3 cm^3/m^2 × 24 h [95]. The ability of the R3PAE active formulation to restrict CO_2 migration down to 4.65 cm^3/m^2 × 24 h without requiring inorganic nanofillers or complex multi-layer coatings underscores the potent structural densification and tortuosity induced by the natural red pomegranate peel polyphenols within the LBG/k-carrageenan network [83,97].

Both low Oxygen Transmission Rate and Carbon Dioxide Transmission Rate are further corroborated by the dense structural packing promoted by E410 and E407 co-constituents.

The salt (10%) and protein (about 7%) components can act as structural domain fillers that effectively plug interstitial micro-cavities within the LBG/k-carrageenan network, drastically lowering gas diffusion coefficients.

3.15. Soil Burial Degradation

The environmental impact and end-of-life assessment of the active bio-packaging film incorporated with the red pomegranate peel aqueous extract (R3PAE) were evaluated through a soil burial degradation assay. Visual monitoring over the 30-day experimental timeframe revealed a good ecocompatibility profile, culminating in the complete breakdown and total macrostructural disappearance of the active matrix within the sieved agricultural soil. It should be noted that gravimetric data were not reported because, after the initial period, the film and its fragments became slightly sticky and adhered to soil particles and debris; consequently, it was impossible to thoroughly clean the samples from the soil and weigh them accurately.

During the first 14 days of the assay, the active formulation underwent progressive moisture absorption from the sieved agricultural soil (pH 7.2, 60% RH), a phenomenon fundamentally driven by the highly hygroscopic nature of the glycerol plasticizer molecules embedded within the matrix. This initial swelling phase expanded the intermolecular spaces of the polymer network, facilitating immediate microbial colonization by the native soil microbiota under climate-controlled conditions (25 °C and 60% RH).

By day 21, extensive macrostructural fragmentation, cracking, and severe structural weakening became visually prominent. This rapid structural collapse is ascribed to the active secretion of extracellular enzymes by soil bacteria and fungi, which targeted and cleaved the primary glycosidic linkages constituting the k-carrageenan/LBG backbone. Crucially, after day 25 and by day 30, the continuous enzymatic digestion and biotic degradation resulted in the complete assimilation of the residual film fragments into the soil matrix, leaving almost no macroscopic residues or polymer aggregates behind (Figure 5).

From an environmental engineering perspective, the complete macrostructural assimilation observed within a 30-day window reflects rapid biotic turnover characteristics of natural hydrocolloid networks [3,44,98]. In soil burial dynamics, the initial plasticizer-driven hydration phase acts as a crucial rate-determining step: glycerol molecules readily absorb soil moisture, expanding the interstitial volume between the galactomannan chains of LBG and the sulfated galactan helices of k-carrageenan [14,76,99]. This matrix swelling enables extracellular hydrolytic enzymes secreted by soil fungi and heterotrophic bacteria to penetrate the hydrocolloid network and cleave the glycosidic bonds [44,82,100].

Importantly, while the incorporation of polyphenolic constituents from R3PAE established a dense non-covalent hydrogen bonding network that provided enhanced mechanical resilience and gas/water vapor barrier protection during the active preservation lifecycle, these physical interactions do not hinder environmental biodegradation [3,18]. Natural polyphenols, predominantly hydrolysable tannins and flavonoids, are inherently biocompatible and probably utilized as carbon sources by soil microbial consortia once released from the matrix [22,23,101]. Unlike conventional petroleum-based plastics or synthetic coatings that persist for decades and fragment into toxic microplastics and nanoplastics, the polysaccharide–polyphenol framework undergoes complete biotic mineralization into biomass, carbon dioxide, and water without leaving persistent chemical residues [1,3,6].

It should be noted that quantitative gravimetric weight loss determination was hindered because the degrading film fragments turned highly soft and sticky during soil burial, as already highlighted, causing soil particles to tightly adhere to the biopolymer matrix and preventing accurate separation without material damage. Although visual monitoring offers

clear qualitative evidence of rapid matrix disintegration, the reliance on visual inspection represents an acknowledged methodological limitation of this soil burial screening.

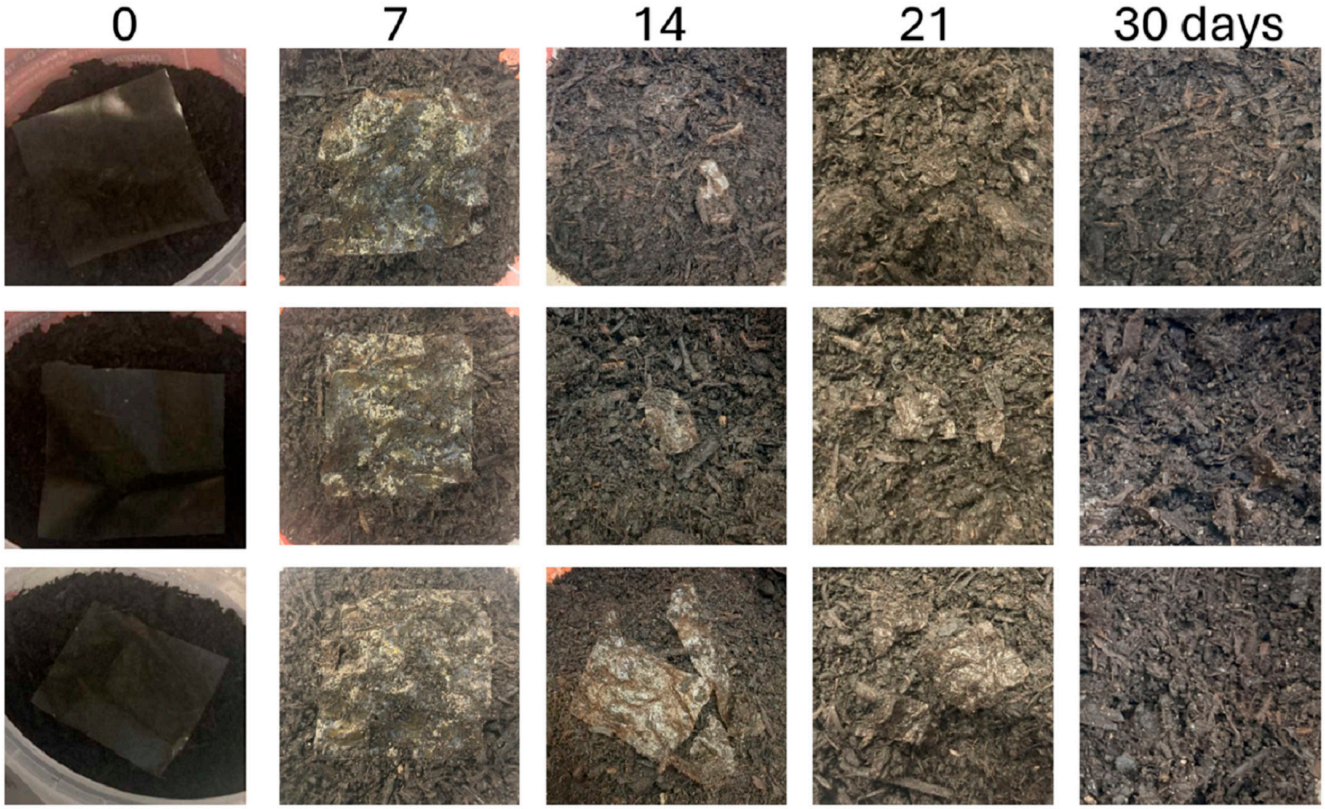


Figure 5. End-of-life assessment of the active bio-packaging film containing red pomegranate peel aqueous extract (R3PAE) during a 30-day soil burial degradation assay monitored by visual observation.

4. Conclusions

This study successfully demonstrates the design, development, and characterization of a novel, fully bio-based active packaging film formulated from commercial carob seed flour (locust bean gum, LBG, E410) and k-carrageenan (E407), plasticized with glycerol and functionalized with red pomegranate peel aqueous extract (R3PAE). Utilizing an eco-friendly, triple sequential ultrasound-assisted extraction protocol with pure water as a green solvent, bioactive constituents were efficiently recovered from agricultural pomegranate peel side-streams. Chromatographic and biochemical profiling confirmed that the resulting extract was highly enriched in phenolic acids, flavonoids, and anthocyanins.

A fundamental finding of this work lies in demonstrating that the strategic utilization of commercial unpurified food-grade additives, containing intrinsic protein, salt, and residual soluble sugar fractions within regulatory legal limits, provides decisive structural and technological advantages over pure biopolymers reported in the literature. These native co-constituents act synergistically: native proteins serve as natural physical crosslinkers and domain fillers, and residual salt and sugars function as dynamic co-plasticizers occupying interstitial free volumes.

The incorporation of R3PAE into the biopolymer matrix conferred effective antimicrobial functionality against both Gram-positive and Gram-negative bacterial pathogens, significantly enhancing film functionality without compromising structural integrity or biodegradability. The multi-hydroxyl active compounds act as polyfunctional physical crosslinkers and domain fillers that heal micro-structural discontinuities formed during film casting. This dual action significantly fortifies tensile strength while remarkably pre-

serving a very good matrix ductility and reducing experimental variability. Concurrently, the combination of physical tortuosity, void filling, and surface hydrophobicity restricts gas and moisture transport, yielding an exceptionally low Water Vapor Transmission Rate and restricted Water Vapor Permeability that directly matches the performance benchmarks of conventional petroleum-derived films, alongside high barrier performance against oxygen and carbon dioxide. Overall, these findings highlight the high potential of valorizing agri-food side-streams into high-value functional bio-packaging materials, directly contributing to a circular bioeconomy and providing a sustainable alternative to fossil-based plastic packaging.

While the present in vitro findings provide a robust proof-of-concept, future research will primarily focus on validating these active films in vivo across real food models. Specifically, storage trials on highly perishable matrices, such as fresh meat, dairy products, and fresh-cut produce, will be conducted to systematically evaluate actual shelf-life extension, microbial growth kinetics, organoleptic/sensory evolution, and film structural stability in direct contact with food. Furthermore, future efforts will address active release kinetics, pilot-scale manufacturing feasibility, standardized respirometric biodegradation testing, and life cycle assessments (LCA) to support commercial viability. Additionally, key aspects preparatory to market translation will be evaluated, including compliance with Food Contact Materials (MOCA) regulations, alignment with the new Packaging and Packaging Waste Regulation (PPWR) requirements, food-grade suitability testing and certifications, as well as the management of intellectual property (IP) protection.

Author Contributions: Conceptualization, G.D.R.; methodology, G.D.R.; software, G.D.R.; validation, G.D.R.; formal analysis, G.D.R.; investigation, G.D.R., G.M., A.D.F., P.R., and C.N.; resources, G.D.R., M.N., V.M., and C.Z.; data curation, G.D.R.; writing—original draft preparation, G.D.R.; writing—review and editing, G.D.R., A.D.F., C.N., and V.M.; visualization, G.D.R.; supervision, V.M.; project administration, G.D.R. and V.M.; funding acquisition, G.D.R., M.N., V.M., and C.Z. All authors have read and agreed to the published version of the manuscript.

Funding: This work was funded within the framework of the METROFOOD-IT Research Infrastructure (Strengthening of the Italian RI for Metrology and Open Access Data in support to the Agrifood), a project that received funding from the NRRP—Mission 4 'Education and Research', Component 2: From Research to Business, Investment 3.1: Fund for the creation of an integrated system of research and innovation infrastructures—IR0000033 (MD No. 120 of 21 June 2022).

Data Availability Statement: The original contributions presented in this study are included in the article. Further inquiries can be directed to the corresponding author.

Acknowledgments: The authors gratefully acknowledge METROFOOD-IT for providing full access to the experimental facilities, pilot equipment, and advanced analytical instrumentation available at the ENEA Research Centers of Brindisi and Casaccia and SUS-MIRRI.IT with the ENEA microbial collection for providing bacterial strains.

Conflicts of Interest: The authors declare no conflicts of interest.

Abbreviations

The following abbreviations are used in this manuscript:

C3G	Cyanidin-3-O-glucoside
CFU	Colony Forming Units
CO2P	Carbon Dioxide Permeability
dRPPPs/RPPP	dried Red Pomegranate Peel Pools/Red Pomegranate Peel Pools
E407	Kappa-carrageenan
EB	Elongation at Break
LBG	Locust Bean Gum

MHA	Mueller–Hinton Agar
MIC	Minimum Inhibitory Concentration
NDIR	Non-Dispersive Infrared
OTR	Oxygen Transmission Rate
QE	Quercetin Equivalents
TAC	Total Anthocyanin Content
TFC	Total Flavonoid Content
UAE	Ultrasound-Assisted Extraction
WL	Weight Loss
WVTR	Water Vapor Transmission Rate
ASTM	American Society for Testing and Materials
ATR-FTIR/FTIR-ATR	Attenuated Total Reflection—Fourier-Transform Infrared Spectroscopy
CE	Catechin Equivalents
CLSI	Clinical and Laboratory Standards Institute
CO2TR	Carbon Dioxide Transmission Rate
DSLR	Digital Single-Lens Reflex
E410	Locust Bean Gum/Carob Seed Flour
GAE	Gallic Acid Equivalents
k-car/k-carrageenan	Kappa-carrageenan
MHB	Mueller–Hinton Broth
OP	Oxygen Permeability
PTFE	Polytetrafluoroethylene
R3PAE	Red Pomegranate Peel Aqueous Extract
TE	Trolox Equivalents
TPC	Total Phenolic Content
WCA	Water Contact Angle
WVP	Water Vapor Permeability

References

1. Marsh, K.; Bugusu, B. Food packaging—Roles, materials, and environmental issues. *J. Food Sci.* **2007**, *72*, R39–R55. [CrossRef] [PubMed]
2. Valdés, A.; Ramos, M.; Beltrán, A.; Jiménez, A.; Garrigós, M.C. State of the Art of Antimicrobial Edible Coatings for Food Packaging Applications. *Coatings* **2017**, *7*, 56. [CrossRef]
3. Siracusa, V.; Rocculi, P.; Romani, S.; Rosa, M.D. Biodegradable polymers for food packaging applications. *Trends Food Sci. Technol.* **2008**, *19*, 634–643. [CrossRef]
4. Gamage, A.; Thiviya, P.; Liyanapathiranage, A.; Wasana, M.L.D.; Jayakodi, Y.; Bandara, A.; Manamperi, A.; Dassanayake, R.S.; Evon, P.; Merah, O.; et al. Polysaccharide-based bioplastics as green and sustainable packaging materials. *J. Compos. Sci.* **2023**, *8*, 413. [CrossRef]
5. Liyanapathiranage, A.; Dassanayake, S.R.; Gamage, A.; Karri, R.R.; Manamperi, A.; Evon, P.; Jayakodi, Y.; Madhujith, T.; Merah, O. Recent developments in edible films and coatings for fruits and vegetables. *Coatings* **2023**, *13*, 1177. [CrossRef]
6. Andrade, M.A.; Barbosa, C.H.; Ribeiro-Santos, R.; Tomé, S.; Fernando, A.L.; Silva, A.S.; Vilarinho, F. Emerging Trends in Active Packaging for Food: A Six-Year Review. *Foods* **2025**, *14*, 2713. [CrossRef] [PubMed]
7. Dos Santos, A.E.; De Matos, F.J.; Monteiro, A.R.; Valencia, G.A. Galactomannans: A Suitable Biopolymer to Produce Advanced Food Packaging. *Int. J. Food Sci.* **2025**, *2025*, 9577986. [CrossRef] [PubMed]
8. Thiviya, P.; Gamage, A.; Liyanapathiranage, A.; Makehelwala, M.; Dassanayake, R.S.; Manamperi, A.; Merah, O.; Mani, S.; Koduru, J.R.; Madhujith, T. Algal polysaccharides: Structure, preparation and applications in food packaging. *Food Chem.* **2023**, *405*, 134903. [CrossRef]
9. Barak, S.; Mudgil, D. Locust bean gum: Processing, properties and food applications-a review. *Int. J. Biol. Macromol.* **2014**, *66*, 74–80. [CrossRef] [PubMed]
10. Singh, S.; Singh, G.; Arya, S.K. Mannans: An overview of properties and application in food products. *Int. J. Biol. Macromol.* **2009**, *119*, 79–95. [CrossRef] [PubMed]
11. Campo, V.L.; Kawano, D.F.; da Silva, D.B.; Carvalho, I. Carrageenans: Biological properties, chemical modifications and structural analysis—A review. *Carbohydr. Polym.* **2009**, *77*, 167–180. [CrossRef]

12. Kokkuvayil, R.B.; Rhim, J.W.; Roy, S. Recent Progress of Carrageenan-Based Composite Films in Active and Intelligent Food Packaging Applications. *Polymers* **2024**, *16*, 1001. [CrossRef] [PubMed]
13. Wang, R.; Zhang, S.; Liu, S.; Sun, Y.; Xu, H. A Contribution to Improve Barrier Properties and Reduce Swelling Ratio of k-Carrageenan Film from the Incorporation of Guar Gum or Locust Bean Gum. *Polymers* **2023**, *15*, 1751. [CrossRef] [PubMed]
14. Martins, J.T.; Cerqueira, M.A.; Bourbon, A.I.; Pinheiro, A.C.; Souza, B.W.S.; Vicente, A.A. Synergistic effects between k-carrageenan and locust bean gum on physicochemical properties of edible films made thereof. *Food Hydrocoll.* **2012**, *29*, 280–289. [CrossRef]
15. Pinheiro, A.C.; Bourbon, A.I.; Rocha, C.; Ribeiro, C.; Maia, J.M.; Gonçalves, M.P.; Teixeira, J.A.; Vicente, A.A. Rheological characterization of k-carrageenan/galactomannan and xanthan/galactomannan gels: Comparison of galactomannans from non-traditional sources with conventional galactomannans. *Carbohyd. Polym.* **2011**, *83*, 392–399. [CrossRef]
16. Spena, S.R.; Pasquino, R.; Grizzuti, N. K-Carrageenan/Locust Bean Gum Gels for Food Applications-A Critical Study on Potential Alternatives to Animal-Based Gelatin. *Foods* **2024**, *13*, 2575. [CrossRef] [PubMed]
17. Abdullah, C.J.; Hafeez, M.A.; Wang, Q.; Farooq, S.; Huang, Q.; Tian, W.; Xiao, J. Biopolymer-based functional films for packaging applications: A review. *Front. Nutr.* **2022**, *9*, 1000116. [CrossRef] [PubMed]
18. Giri, N.A.; Gaikwad, N.N.; Raigond, P.; Damale, R.; Marathe, R.A. Exploring the potential of pomegranate peel extract as a natural food additive: A review. *Curr. Nutr. Rep.* **2023**, *12*, 270–289. [CrossRef] [PubMed]
19. Moussaoui, B.; Rahali, A.; Hanafi, T.; Guemoud, L.; Zemour, K.; Riazi, A.; Merah, O.; Halis, S.; Hassouni, I. Development and characterization of active edible *Opuntia* mucilage/locust bean gum packaging incorporated with *Opuntia* cladodes polyphenols. *Appl. Food Res.* **2025**, *5*, 101218. [CrossRef]
20. El-Hamamsy, S.M.A.; El-khamissi, H.A.Z. Phytochemicals, antioxidant activity and identification of phenolic compounds by HPLC of pomegranate (*Punica granatum* L.) peel extracts. *J. Agric. Chem. Biotechnol.* **2020**, *11*, 79–84. [CrossRef]
21. Montefusco, A.; Durante, M.; Migoni, D.; De Caroli, M.; Ilahy, R.; Pék, Z.; Helyes, L.; Fanizzi, F.P.; Mita, G.; Piro, G.; et al. Analysis of the Phytochemical Composition of Pomegranate Fruit Juices, Peels and Kernels: A Comparative Study on Four Cultivars Grown in Southern Italy. *Plants* **2021**, *10*, 2521. [CrossRef] [PubMed]
22. Azmat, F.; Safdar, M.; Ahmad, H.; Khan, M.R.J.; Abid, J.; Naseer, M.S.; Aggarwal, S.; Imran, A.; Khalid, U.; Zahra, M.S.; et al. Phytochemical profile, nutritional composition of pomegranate peel and peel extract as a potential source of nutraceutical: A comprehensive review. *Food Sci. Nutr.* **2024**, *12*, 661–674. [CrossRef] [PubMed]
23. Salim, A.; Deiana, P.; Fancello, F.; Molinu, M.G.; Santona, M.; Zara, S. Antimicrobial and antibiofilm activities of pomegranate peel phenolic compounds: Varietal screening through a multivariate approach. *J. Bioresour. Bioprod.* **2023**, *8*, 146–161. [CrossRef]
24. Chemat, F.; Rombaut, N.; Sicaire, A.G.; Meullemiestre, A.; Fabiano-Tixier, A.S.; Abert-Vian, M. Ultrasound assisted extraction of food and natural products. Mechanisms, techniques, combinations, protocols and applications. A review. *Ultrason. Sonochem.* **2017**, *34*, 540–560. [CrossRef] [PubMed]
25. Aragón-Gutiérrez, A.; Rosa, E.; Gallur, M.; López, D.; Hernández-Muñoz, P.; Gavara, R. Melt-processed bioactive EVOH films incorporated with ferulic acid. *Polymers* **2020**, *13*, 68. [CrossRef] [PubMed]
26. Mphahlele, R.R.; Fawole, O.A.; Makunga, N.P.; Opara, U.L. Effect of drying on the bioactive compounds, antioxidant, antibacterial and antityrosinase activities of pomegranate peel. *BMC Complement. Altern. Med.* **2016**, *16*, 143. [CrossRef] [PubMed]
27. Al-Dhabi, N.A.; Ponmurugan, K.; Jeganathan, P.M. Development and validation of ultrasound-assisted solid-liquid extraction of phenolic compounds from waste spent coffee grounds. *Ultrason. Sonochem.* **2017**, *34*, 206–213. [CrossRef] [PubMed]
28. Pan, Z.; Qu, W.; Ma, H.; Atungulu, G.G.; McHugh, T.H. Continuous and pulsed ultrasound-assisted extractions of antioxidants from pomegranate peel. *Ultrason. Sonochem.* **2011**, *18*, 1249–1257. [CrossRef] [PubMed]
29. Kaderides, K.; Papaoikonomou, L.; Serafim, M.; Goula, A.M. Microwave-assisted extraction of phenolics from pomegranate peels: Optimization, kinetics, and comparison with ultrasounds extraction. *Chem. Eng. Process. Process Intensif.* **2019**, *137*, 1–11. [CrossRef]
30. Luque-Rodríguez, J.M.; Pérez-Juan, P.; de Castro, M.D.L. Extraction of polyphenols from vine shoots of *Vitis vinifera* by superheated ethanol–water mixtures. *J. Agric. Food Chem.* **2006**, *54*, 8775–8781. [CrossRef] [PubMed]
31. Emmons, C.L.; Peterson, D.M.; Paul, G.L. Antioxidant capacity of oat (*Avena sativa* L.) extracts. 2. In Vitro antioxidant activity and contents of phenolic and tocol antioxidants. *J. Agric. Food Chem.* **1999**, *47*, 4894–4898. [CrossRef] [PubMed]
32. Win, A.; Nyo, A.M.T.; Lwin, K.M. Determination of total flavonoid content of commonly consumed commercial tea. *Int. J. Sci. Res. Publ.* **2019**, *9*, 802–808. [CrossRef]
33. Iland, P.G.; Cynkar, W.; Francis, I.L.; Williams, P.J.; Coombe, B.G. Optimisation of methods for the determination of total and red-free glycosyl glucose in black grape berries of *Vitis vinifera*. *Aust. J. Grape Wine Res.* **1996**, *2*, 171–178. [CrossRef]
34. Li, D.; Li, X.; Ding, X. Composition and antioxidative properties of the flavonoid-rich fractions from tartary buckwheat grains. *Food Sci. Biotechnol.* **2010**, *19*, 711–716. [CrossRef]
35. Elshikh, M.; Ahmed, S.; Funston, S.; Dunlop, P.; McGaw, M.; Marchant, R.; Banat, I.M. Resazurin-based 96-well plate microdilution method for the determination of minimum inhibitory concentration of biosurfactants. *Biotechnol. Lett.* **2016**, *38*, 1015–1019. [CrossRef] [PubMed]

36. Bauer, A.W.; Kirby, W.M.M.; Sherris, J.C.; Turck, M. Antibiotic susceptibility testing by a standardized single disk method. *Am. J. Clin. Pathol.* **1966**, *45*, 493–496. [CrossRef]
37. Baümler, E.R.; Cuniberti, A.M.; Nolasco, S.M.; Riccobene, I.C. Moisture dependent physical and compression properties of safflower seed. *J. Food Eng.* **2006**, *72*, 134–140. [CrossRef]
38. *ASTM D882-18*; Standard Test Method for Tensile Properties of Thin Plastic Sheeting. ASTM International: West Conshohocken, PA, USA, 2018.
39. *ASTM D7334-08*; Standard Practice for Surface Wettability of Coatings, Substrates and Pigments by Advancing Contact Angle Measurement. ASTM International: West Conshohocken, PA, USA, 2022.
40. Brugnara, M. Contact Angle Plugin (for ImageJ Software, Version 1.54t 16 May 2026). Image Processing and Analysis in Java 2006. Available online: https://imagej.net/ij/plugins/contact-angle.html (accessed on 27 October 2026).
41. *ASTM F1249-20*; Standard Test Method for Water Vapor Transmission Rate Through Plastic Film and Sheeting Using a Modulated Infrared Sensor. ASTM International: West Conshohocken, PA, USA, 2020.
42. *ASTM F2476-20*; Standard Test Method for the Determination of Carbon Dioxide Gas Transmission Rate (CO2TR) Through Barrier Materials Using an Infrared Detector. ASTM International: West Conshohocken, PA, USA, 2020.
43. *ASTM D3985-24*; Standard Test Method for Oxygen Gas Transmission Rate Through Plastic Film and Sheeting Using a Coulometric Sensor. ASTM International: West Conshohocken, PA, USA, 2024.
44. de Oliveira Alves, L.T.; Fronza, P.; Gonçalves, I.; da Silva, W.A.; Oliveira, L.S.; Franca, A.S. Development of Polymeric Films Based on Sunflower Seed Proteins and Locust Bean Gum. *Polymers* **2024**, *16*, 1905. [CrossRef] [PubMed]
45. Fawole, O.; Opara, U.L. Composition of trace and major minerals in different parts of pomegranate (*Punica granatum*) fruit cultivars. *Br. Food J.* **2012**, *114*, 1518–1532. [CrossRef]
46. Kumar, K.; Srivastav, S.; Sharanagat, V.S. Ultrasound assisted extraction (UAE) of bioactive compounds from fruit and vegetable processing by-products: A review. *Ultrason. Sonochem.* **2021**, *70*, 105325. [CrossRef] [PubMed]
47. Toledo-Merma, P.R.; Cornejo-Figueroa, M.H.; Crisosto-Fuster, A.d.R.; Strieder, M.M.; Chañi-Paucar, L.O.; Náthia-Neves, G.; Rodríguez-Papuico, H.; Rostagno, M.A.; Meireles, M.A.A.; Alcázar-Alay, S.C. Phenolic Compounds Recovery from Pomegranate (*Punica granatum* L.) By-Products of Pressurized Liquid Extraction. *Foods* **2022**, *11*, 1070. [CrossRef] [PubMed]
48. Mehta, N.; S, J.; Kumar, P.; Verma, A.K.; Umaraw, P.; Khatkar, S.K.; Khatkar, A.B.; Pathak, D.; Kaka, U.; Sazili, A.Q. Ultrasound-Assisted Extraction and the Encapsulation of Bioactive Components for Food Applications. *Foods* **2022**, *11*, 2973. [CrossRef] [PubMed]
49. Aimone, C.; Grillo, G.; Boffa, L.; Giovando, S.; Cravotto, G. Tannin Extraction from Chestnut Wood Waste: From Lab Scale to Semi-Industrial Plant. *Appl. Sci.* **2023**, *13*, 2494. [CrossRef]
50. Withouck, H.; Paelinck, A.; Foubert, I.; Fraeye, I. Ultrasound-Assisted Extraction of Applewood Polyphenols at Lab and Pilot Scales. *Foods* **2023**, *12*, 3142. [CrossRef] [PubMed]
51. Fischer, U.A.; Carle, R.; Kammerer, D.R. Identification and quantification of phenolic compounds in pomegranate (*Punica granatum* L.) peel, mesocarp, aril and differently pressed juices by HPLC-DAD-ESI/MS^n. *Food Chem.* **2011**, *127*, 807–821. [CrossRef] [PubMed]
52. Lampakis, D.; Skenderidis, P.; Leontopoulos, S. Technologies and Extraction Methods of Polyphenolic Compounds Derived from Pomegranate (*Punica granatum*) Peels. A Mini Review. *Processes* **2021**, *9*, 236. [CrossRef]
53. Akhtar, S.; Ismail, T.; Fraternale, D.; Sestili, P. Pomegranate peel and peel extracts: Chemistry and food features. *Food Chem.* **2015**, *174*, 417–425. [CrossRef] [PubMed]
54. Shehzadi, F.; Shoaib, M.; Munir, S.; Abdi, G. Ultrasound-assisted extraction of bioactive compounds from pomegranate peel and seed: A comprehensive review of key parameters and optimization strategies. *Ultrason. Sonochem.* **2026**, *124*, 107722. [CrossRef] [PubMed]
55. Ismail, T.; Sestili, P.; Akhtar, S. Pomegranate peel and fruit extracts: A review of potential anti-inflammatory and anti-infective effects. *J. Ethnopharmacol.* **2012**, *143*, 397–405. [CrossRef] [PubMed]
56. Palomino, J.C.; Martin, A.; Camacho, M.; Guerra, H.; Swings, J.; Portaels, F. Resazurin microplate assay: Simple and inexpensive method for detection of drug resistance in *Mycobacterium tuberculosis*. *Antimicrob. Agents Chemother.* **2002**, *46*, 2720–2722. [CrossRef] [PubMed]
57. Sarker, S.D.; Nahar, L.; Kumarasamy, Y. Microtitre plate-based antibacterial assay incorporating resazurin as an indicator of cell growth, and its application in the in vitro antibacterial screening of phytochemicals. *Methods* **2007**, *42*, 321–324. [CrossRef] [PubMed]
58. Mann, C.M.; Markham, J.L. A new method for determining the minimum inhibitory concentration of essential oils. *J. Appl. Microbiol.* **1998**, *84*, 538–544. [CrossRef] [PubMed]
59. Maher, C.; Hassan, K.A. The Gram-negative permeability barrier: Tipping the balance of the in and the out. *mBio* **2023**, *14*, e01205-23. [CrossRef] [PubMed]

60. Alegun, O.; Pandeya, A.; Cui, J.; Ojo, I.; Wei, Y. Donnan Potential across the Outer Membrane of Gram-Negative Bacteria and Its Effect on the Permeability of Antibiotics. *Antibiotics* **2021**, *10*, 701. [CrossRef] [PubMed]
61. Miklasińska-Majdanik, M.; Kępa, M.; Wojtyczka, R.D.; Idzik, D.; Wąsik, T.J. Phenolic Compounds Diminish Antibiotic Resistance of *Staphylococcus aureus* Clinical Strains. *Int. J. Environ. Res. Public Health* **2018**, *15*, 2321. [CrossRef] [PubMed]
62. Takó, M.; Kerekes, E.B.; Zambrano, C.; Kotogán, A.; Papp, T.; Krisch, J.; Vágvölgyi, C. Plant Phenolics and Phenolic-Enriched Extracts as Antimicrobial Agents against Food-Contaminating Microorganisms. *Antioxidants* **2020**, *9*, 165. [CrossRef] [PubMed]
63. Balouiri, M.; Sadiki, M.; Ibnsouda, S.K. Methods for in vitro evaluating antimicrobial activity: A review. *J. Pharm. Anal.* **2016**, *6*, 71–79. [CrossRef] [PubMed]
64. CLSI. *Performance Standards for Antimicrobial Disk Susceptibility Tests* , 13th ed.; M02; Clinical and Laboratory Standards Institute: Wayne, PA, USA, 2018. Available online: https://clsi.org/shop/standards/m02/ (accessed on 27 October 2026).
65. Nuamsetti, T.; Dechayuenyong, P.; Tantipaibulvut, S. Antibacterial activity of pomegranate fruit peels and arils. *Sci. Asia* **2012**, *38*, 319–322. [CrossRef]
66. Kupnik, K.; Primožič, M.; Vasić, K.; Knez, Ž.; Leitgeb, M. A Comprehensive Study of the Antibacterial Activity of Bioactive Juice and Extracts from Pomegranate (*Punica granatum* L.) Peels and Seeds. *Plants* **2021**, *10*, 1554. [CrossRef] [PubMed]
67. Breijyeh, Z.; Jubeh, B.; Karaman, R. Resistance of Gram-Negative Bacteria to Current Antibacterial Agents and Approaches to Resolve It. *Molecules* **2020**, *25*, 1340. [CrossRef] [PubMed]
68. Devatkal, S.K.; Jaiswal, P.; Jha, S.N.; Bharadwaj, R.; Viswas, K.N. Antibacterial activity of aqueous extract of pomegranate peel against *Pseudomonas stutzeri* isolated from poultry meat. *J. Food Sci. Technol.* **2011**, *50*, 555–560. [CrossRef] [PubMed]
69. Abu-Niaaj, L.F.; Al-Daghistani, H.I.; Katampe, I.; Abu-Irmaileh, B.; Bustanji, Y.K. Pomegranate peel: Bioactivities as antimicrobial and cytotoxic agents. *Food Sci. Nutr.* **2024**, *12*, 2818–2832. [CrossRef] [PubMed]
70. Mendes, P.M.; Fontoura, G.M.G.; dos Santos Rodrigues, L.; Souza, A.S.; Viana, J.P.M.; Pereira, A.L.F.; Dutra, R.P.; Ferreira, A.G.N.; Neto, M.S.; Reis, A.S.; et al. Therapeutic Potential of *Punica granatum* and Isolated Compounds: Evidence-Based Advances to Treat Bacterial Infections. *Int. J. Microbiol.* **2023**, *2023*, 4026440. [CrossRef] [PubMed]
71. Salgado, P.R.; Ortiz, C.M.; Musso, Y.S.; Di Giorgio, L.; Mauri, A.N. Edible films and coatings containing bio-actives. *Curr. Opin. Food Sci.* **2015**, *5*, 86–92. [CrossRef]
72. Piculell, L.; Zhang, W.; Turquois, T.; Rochas, C.; Taravel, F.R.; Williams, P.A. Effects of added galacto- and gluco-mannans on the NMR spectra of 133CS ions in kappa-carrageenan gels. *Carbohydr. Res.* **1994**, *265*, 281–290. [CrossRef]
73. Riahi, Z.; Priyadarshi, R.; Rhim, J.W.; Bagheri, R. Gelatin-based functional films integrated with grapefruit seed extract and TiO_2 for active food packaging applications. *Food Hydrocoll.* **2021**, *112*, 106314. [CrossRef]
74. Antosik, A.K.; Kowalska, U.; Stobińska, M.; Dzięcioł, P.; Pieczykolan, M.; Kozłowska, K.; Bartkowiak, A. Development and Characterization of Bioactive Polypropylene Films for Food Packaging Applications. *Polymers* **2021**, *13*, 3478. [CrossRef] [PubMed]
75. Al-Hassan, A.A.; Norziah, M.H. Starch–gelatin edible films: Water vapor permeability and mechanical properties as affected by plasticizers. *Food Hydrocoll.* **2012**, *26*, 108–117. [CrossRef]
76. Qin, Y.; Liu, Y.; Zhang, X.; Liu, J. Development of active and intelligent packaging by incorporating betalains from red pitaya (*Hylocereus polyrhizus*) peel into starch/polyvinyl alcohol films. *Food Hydrocoll.* **2020**, *100*, 105410. [CrossRef]
77. Cushnie, T.P.T.; Lamb, A.J. Recent advances in understanding the antibacterial properties of flavonoids. *Int. J. Antimicrob. Agents* **2011**, *38*, 99–107. [CrossRef] [PubMed]
78. Ghai, I.; Ghai, S. Understanding antibiotic resistance via outer membrane permeability. *Infect. Drug Resist.* **2018**, *11*, 523–530. [CrossRef] [PubMed]
79. Siripatrawan, U.; Harte, B.R. Physical properties and antioxidant activity of active packaging films based on chitosan incorporated with green tea extract. *Food Hydrocoll.* **2010**, *24*, 770–775. [CrossRef]
80. Zhang, W.; Rhim, J.W. Recent progress in konjac glucomannan-based active food packaging films and property enhancement strategies. *Food Hydrocoll.* **2022**, *128*, 107572. [CrossRef]
81. Kanmani, P.; Rhim, J.W. Development and characterization of carrageenan/grapefruit seed extract composite films for active packaging. *Int. J. Biol. Macromol.* **2014**, *68*, 258–266. [CrossRef] [PubMed]
82. Rhim, J.W.; Park, H.M.; Ha, C.S. Bio-nanocomposites for food packaging applications. *Prog. Polym. Sci.* **2013**, *38*, 1629–1652. [CrossRef]
83. Avila, L.B.; Barreto, E.R.C.; Moraes, C.C.; Morais, M.M.; da Rosa, G.S. Promising New Material for Food Packaging: An Active and Intelligent Carrageenan Film with Natural Jaboticaba Additive. *Foods* **2022**, *11*, 792. [CrossRef] [PubMed]
84. Faria, C.S.V.; Vieira, J.M.; Vicente, A.A.; Martins, J.T. Locust Bean Gum/κ-Carrageenan Film Containing Blueberry or Beetroot Extracts as Intelligent Films to Monitoring Hake (*Merluccius merluccius*) Freshness. *Foods* **2024**, *13*, 3088. [CrossRef] [PubMed]
85. Cerqueira, M.A.; Souza, B.W.S.; Teixeira, J.A.; Vicente, A.A. Effect of glycerol and corn oil on physicochemical properties of polysaccharide films—A comparative study. *Food Hydrocoll.* **2012**, *27*, 175–184. [CrossRef]
86. Jouki, M.; Mortazavi, S.A.; Yazdi, F.T.; Koocheki, A. Characterization of antioxidant–antibacterial quince seed mucilage films containing thyme essential oil. *Carbohydr. Polym.* **2014**, *99*, 537–546. [CrossRef] [PubMed]

87. Sedayu, B.B.; Cran, M.J.; Bigger, S.W. Characterization of Semi-refined Carrageenan-Based Film for Primary Food Packaging Purposes. *J. Polym. Environ.* **2018**, *26*, 3754–3761. [CrossRef]
88. Vogler, E.A. Water and the acute biological response to surfaces. *J. Biomater. Sci. Polym. Ed.* **1999**, *10*, 1015–1045. [CrossRef] [PubMed]
89. Yuan, Y.; Lee, T.R. Contact Angle and Wetting Properties. In *Surface Science Techniques*; Bracco, G., Holst, B., Eds.; Springer Series in Surface Sciences; Springer: Berlin/Heidelberg, Germany, 2013; Volume 51, pp. 3–34. [CrossRef]
90. Helmy, M.M.; Younes, O.S.; Sorour, M.A. Effect of Drying Methods on Edible Film Properties. *Middle East J. Appl. Sci.* **2019**, *9*, 1168–1176. [CrossRef]
91. Galus, S.; Kadzińska, J. Food applications of emulsion-based edible films and coatings. *Trends Food Sci. Technol.* **2015**, *45*, 273–283. [CrossRef]
92. Vieira, M.G.A.; da Silva, M.A.; dos Santos, L.O.; Beppu, M.M. Natural-based plasticizers and biopolymer films: A review. *Eur. Polym. J.* **2011**, *47*, 254–263. [CrossRef]
93. Kanatt, S.R.; Rao, M.S.; Chawla, S.P.; Sharma, A. Active chitosan–polyvinyl alcohol films with natural extracts. *Food Hydrocoll.* **2012**, *29*, 290–297. [CrossRef]
94. Saidi, L.; Hosseini, M.; Spicer, P.T.; Wang, Y.; Wich, P.R.; Selomulya, C. Impact of Polyphenols on Water Vapor Barrier in Carboxymethyl Cellulose Films Reinforced with Bacterial Cellulose Nanofibers. *Food Bioprocess Technol.* **2026**, *19*, 228. [CrossRef]
95. Lazić, V.; Vivod, V.; Peršin, Z.; Stoiljković, M.; Ratnayake, I.S.; Ahrenkiel, P.S.; Nedeljković, J.M.; Kokol, V. Dextran-coated silver nanoparticles for improved barrier and controlled antimicrobial properties of nanocellulose films used in food packaging. *Food Packag. Shelf Life* **2020**, *26*, 100575. [CrossRef]
96. Stefanowska, K.; Bucher, M.; Reichert, C.L.; Sip, A.; Woźniak, M.; Schmid, M.; Dobrucka, R.; Ratajczak, I. Chitosan-based films with nanocellulose and propolis as active packaging materials. *Ind. Crops Prod.* **2024**, *219*, 119112. [CrossRef]
97. Gülen, R.B. *Hypericum scabrum* L.-infused locust bean gum/agar hydrogel film: A novel candidate for anti-aging facial mask applications. *Int. J. Biol. Macromol.* **2025**, *306*, 141673. [CrossRef] [PubMed]
98. Fronza, P.; Batista, M.J.P.A.; Franca, A.S.; Oliveira, L.S. Bionanocomposite Based on Cassava Waste Starch, Locust Bean Galactomannan, and Cassava Waste Cellulose Nanofibers. *Foods* **2024**, *13*, 202. [CrossRef] [PubMed]
99. Chen, Y.; Guo, J.; Alamri, A.S.; Alhomrani, M.; Huang, Z.; Zhang, W. Recent research progress on locust bean gum (LBG)-based composite films for food packaging. *Carbohydr. Polym.* **2024**, *348*, 122815. [CrossRef] [PubMed]
100. Malekzadeh, E.; Tatari, A.; Firouzabadi, M.D. Effects of biodegradation of starch-nanocellulose films incorporated with black tea extract on soil quality. *Sci. Rep.* **2024**, *14*, 18817. [CrossRef] [PubMed]
101. Biolchini, M.; Araniti, F.; Abenavoli, M.R.; Sorgonà, A. Flavonoids influence key rhizocompetence traits for early root colonization and can serve as carbon sources for soil microbial communities. *Front. Plant Sci.* **2024**, *15*, 1325048. [CrossRef] [PubMed]

Disclaimer/Publisher's Note: The statements, opinions and data contained in all publications are solely those of the individual author(s) and contributor(s) and not of MDPI and/or the editor(s). MDPI and/or the editor(s) disclaim responsibility for any injury to people or property resulting from any ideas, methods, instructions or products referred to in the content.